ISSN 2444-4987

Journal of Research and Development

Volume 8, Issue 21 – January – June – 2022

ECORFAN®

Journal of Research and Development, Volume 8, Number 21, June - 2022, is a sixmonthly Journal edited by ECORFAN-Spain. Matacerquillas Street 38, CP: 28411. Moralzarzal - Madrid. WEB: http://www.ecorfan.org/spain/rj_investigacion_d.php, revista@ecorfan.org. Editor in Chief: VARGAS-DELGADO, Oscar. PhD. ISSN 2444-4987. Responsible for the last update of this issue ECORFAN Computer Unit. Escamilla Bouchán-Imelda, Luna Soto-Vladimir, updated to June 30, 2022.

Journal of Research and Development

Definition of Journal

Scientific Objectives

Support the international scientific community in its written production Science, Technology and Innovation in the Field of Humanities and Behavioral Sciences, in Subdisciplines of industrial development, project model, computer application, research production, systems development, research networks, application design, programming and development proposals.

ECORFAN-Mexico SC is a Scientific and Technological Company in contribution to the Human Resource training focused on the continuity in the critical analysis of International Research and is attached to CONACYT-RENIECYT number 1702902, its commitment is to disseminate research and contributions of the International Scientific Community, academic institutions, agencies and entities of the public and private sectors and contribute to the linking of researchers who carry out scientific activities, technological developments and training of specialized human resources with governments, companies and social organizations.

Encourage the interlocution of the International Scientific Community with other Study Centers in Mexico and abroad and promote a wide incorporation of academics, specialists and researchers to the publication in Science Structures of Autonomous Universities - State Public Universities - Federal IES - Polytechnic Universities - Technological Universities - Federal Technological Institutes - Normal Schools - Decentralized Technological Institutes - Intercultural Universities - S & T Councils - CONACYT Research Centers.

Scope, Coverage and Audience

Journal of Research and Development is a Journal edited by ECORFAN-Mexico S.C in its Holding with repository in Spain, is a scientific publication arbitrated and indexed with semester periods. It supports a wide range of contents that are evaluated by academic peers by the Double-Blind method, around subjects related to the theory and practice of industrial development, project model, computer application, research production, systems development, research networks, application design, programming and development proposals with diverse approaches and perspectives , That contribute to the diffusion of the development of Science Technology and Innovation that allow the arguments related to the decision making and influence in the formulation of international policies in the Field of Humanities and Behavioral Sciences. The editorial horizon of ECORFAN-Mexico® extends beyond the academy and integrates other segments of research and analysis outside the scope, as long as they meet the requirements of rigorous argumentative and scientific, as well as addressing issues of general and current interest of the International Scientific Society.

Editorial Board

Arbitration Committee

Assignment of Rights

The sending of an Article to Journal of Research and Development emanates the commitment of the author not to submit it simultaneously to the consideration of other series publications for it must complement the Originality Format for its Article.

The authors sign the Authorization Format for their Article to be disseminated by means that ECORFAN-Mexico, S.C. In its Holding Spain considers pertinent for disclosure and diffusion of its Article its Rights of Work.

Declaration of Authorship

Indicate the Name of Author and Coauthors at most in the participation of the Article and indicate in extensive the Institutional Affiliation indicating the Department.

Identify the Name of Author and Coauthors at most with the CVU Scholarship Number-PNPC or SNI-CONACYT- Indicating the Researcher Level and their Google Scholar Profile to verify their Citation Level and H index.

Identify the Name of Author and Coauthors at most in the Science and Technology Profiles widely accepted by the International Scientific Community ORC ID - Researcher ID Thomson - arXiv Author ID - PubMed Author ID - Open ID respectively.

Indicate the contact for correspondence to the Author (Mail and Telephone) and indicate the Researcher who contributes as the first Author of the Article.

Plagiarism Detection

All Articles will be tested by plagiarism software PLAGSCAN if a plagiarism level is detected Positive will not be sent to arbitration and will be rescinded of the reception of the Article notifying the Authors responsible, claiming that academic plagiarism is criminalized in the Penal Code.

Arbitration Process

All Articles will be evaluated by academic peers by the Double Blind method, the Arbitration Approval is a requirement for the Editorial Board to make a final decision that will be final in all cases. MARVID® is a derivative brand of ECORFAN® specialized in providing the expert evaluators all of them with Doctorate degree and distinction of International Researchers in the respective Councils of Science and Technology the counterpart of CONACYT for the chapters of America-Europe-Asia- Africa and Oceania. The identification of the authorship should only appear on a first removable page, in order to ensure that the Arbitration process is anonymous and covers the following stages: Identification of the Journal with its author occupation rate - Identification of Authors and Coauthors - Detection of plagiarism PLAGSCAN - Review of Formats of Authorization and Originality-Allocation to the Editorial Board-Allocation of the pair of Expert Arbitrators-Notification of Arbitration -Declaration of observations to the Author-Verification of Article Modified for Editing-Publication.

Instructions for Scientific, Technological and Innovation Publication

Knowledge Area

The works must be unpublished and refer to topics of industrial development, project model, computer application, research production, systems development, research networks, application design, programming and development proposals and other topics related to Humanities and Behavioral Sciences.

Presentation of the Content

In the first article we present, *Analysis of wear for a base Steel 5% Cr, applying 392 N of load and variable speed of 0.18 m/s, 0.36 m/s and 0.54 m/s, using the T05 Block-on-ring wear tester machine*, by OROZCO-GARCÍA, Calvin Jacob, SERVIN-CASTAÑEDA, Rumualdo, SAN MIGUEL-IZA, Sandra María and GONZÁLEZ-ZARAZUA, Roberto Aldo, with ascription in the UAdeC and Universidad Tecnológica de la Región Centro de Coahuila, as the next article we present, *Design process for dual coplanar waveguide directional couplers for power transmission*, by CASTAÑEDA-IBARRA, Víctor R., CISNEROS-SINENCIO, Luis F., GARCÍA-VITE, Pedro M. and CASTILLO-GUTIÉRREZ, Rafael, with ascription in the, Instituto Tecnológico de Ciudad Madero, as the next article we present, *Assessment of an organic Rankine cycle and a Kalina cycle for a single source of low-enthalpy geothermal heat*, by VERA-ROMERO, Iván, MARTÍNEZ-REYES, José and MÉNDEZ-ÁBREGO, V. Manuel, with ascription in the Universidad de la Ciénega del Estado de Michoacán de Ocampo, as the last article we present, *Design and automation of an electrospinning system to prepare micro and nanofibers. Case study: elaboration of polymeric micro and nanofibers for vaginal drug delivery*, by MARTÍNEZ-PÉREZ, Beatriz, OLIVANO-ESQUIVEL, Ana Daniela, FERNÁNDEZ-RETANA, Jorge and VIDAL-ROMERO, Gustavo, with ascription in the Universidad Politécnica del Valle de México and Universidad Nacional Autónoma de México.

Content

Article **Journal of Research and Development**
June 2022 Vol.8 No.21 1-5

Analysis of wear for a base Steel 5% Cr, applying 392 N of load and variable speed of 0.18 m/s, 0.36 m/s and 0.54 m/s, using the T05 Block-on-ring wear tester machine

Análisis de desgaste para un acero base 5% Cr, aplicando carga de 392 N y velocidad variable de 0.18 m/s, 0.36 m/s y 0.54 m/s, utilizando la máquina de prueba de desgaste T05 Block-on-ring

OROZCO-GARCÍA, Calvin Jacob†´, SERVIN-CASTAÑEDA, Rumualdo*´´, SAN MIGUEL-IZA, Sandra Maria´´´ and GONZÁLEZ-ZARAZUA, Roberto Aldo´´´

´ Facultad de Metalurgia – UAdeC, Carretera 57 Km 5 Norte, C.P 25710 Monclova Coahuila, México.
´´ Facultad de Ingeniería Mecánica y Eléctrica – UAdeC. Barranquilla S/N, Colonia Guadalupe, C.P 257500 Monclova Coahuila. México.
´´´ Universidad Tecnológica de la Región Centro de Coahuila. Carretera 57 Nte Km 14.5, Tramo Monclova-Sabinas, Monclova Coahuila, México.

ID 1st Author: *Calvin Jacob, Orozco-Garcia* / **ORC ID:** 0000-0002-5841-2441, **CVU CONACYT ID:** 1100408

ID 1st Co-author: *Rumualdo, Servin-Castañeda* / **ORC ID:** 0000-0002-8655-2572, **CVU CONACYT ID:** 45820

ID 2nd Co-author: *Sandra Maria, San Miguel-Iza* / **ORC ID:** 0000-0002-3012-3250, **CVU CONACYT ID:** 440841

ID 3rd Co-author: *Roberto Aldo, Gonzalez-Zarazua* / **ORC ID:** 0000-0002-7597-3697, **CVU CONACYT ID:** 254740

DOI: 10.35429/JRD.2022.21.8.1.5 Received: January 20, 2022; Accepted: April 30, 2022

Abstract

In the present study, an experimental analysis of the friction forces, speeds and friction coefficients that influence the size of the wear track in a steel exposed to mechanical contact was carried out, for this, steel blocks with an alloying element of. 5% Cr base and D2 steel standard ring, representing the Block-on-Disk method, according to the ASTM D2714 standard were used. The test parameters were: 392N load, for 800 seconds, with variable speeds of 0.18 m/sec, 0.36 m/sec and 0.54 m/sec; the test is performed in a dry environment using the T-05 Block-on-Ring wear tester machine. This analysis contributes to the technological development of a material that has a lower coefficient of friction and therefore improves its mechanical properties for systems exposed to this principle, such as the wheels of traveling cranes or railway trains, diesel machinery transport systems and various services, etc.

Friction, Wear, Block-on-Disk

Resumen

En el presente estudio se realiza un análisis experimental de las fuerzas de fricción, velocidades y coeficientes de fricción que influyen en el tamaño de la huella de desgaste en un acero expuesto a contacto mecánico, para ello se utilizaron bloques de acero con un elemento de aleación base de 5% de Cr y anillo patron de acero D2, representando el método Block-on-Disk, de acuerdo con la norma ASTM D2714. Los parámetros de prueba fueron: 392N de carga, durante 800 segundos, con velocidades variables de 0.18 m/seg, 0.36 m/seg y 0.54 m/seg; el ensayo se realiza en un ambiente seco utilizando la máquina de desgaste T-05 Block-on-Ring. Con este análisis se está contribuyendo a desarrollar tecnológicamente un material que tenga un coeficiente de fricción menor y por consiguiente mejore sus propiedades mecánicas para sistemas expuestos con este principió, tales como las ruedas de las grúas viajeras o trenes de ferrocarril, sistemas de transporte de maquinaria diesel y servicios diversos, etc.

Fricción, Desgaste, Block-on-Disk

Citation: OROZCO-GARCÍA, Calvin Jacob, SERVIN-CASTAÑEDA, Rumualdo, SAN MIGUEL-IZA, Sandra María and GONZÁLEZ-ZARAZUA, Roberto Aldo. Analysis of wear for a base Steel 5% Cr, applying 392 N of load and variable speed of 0.18 m/s, 0.36 m/s and 0.54 m/s, using the T05 Block-on-ring wear tester machine. Journal of Research and Development. 2022. 8-21:1-5.

* Correspondence to the Author (E-mail: rumualdo.servin@uadec.edu.mx)
† Researcher contributing as first author.

Introduction

Wear is an inevitable phenomenon that occurs whenever two surfaces interact. Normally, wear does not cause violent failures, but it generates functional consequences such as reduced efficiency, higher energy consumption, power losses and the generation of heat from the components, due to the increase in friction coefficients. In recent decades, there has been a growing interest in the subject of friction and wear, and considerable effort has been put into determining its causes and how to prevent its consequences.

Wirokanupatum S. (1999), performs wear tests, where he compares the abrasion phenomenon in dry and wet condition, in a medium carbon steel, confirming that the wear and friction coefficient changes when the operational parameters such as: load, size, shape and abrasive hardness are changed.

Deuis et Al (1998), performs a comparison between the behavior of the friction coefficient in a dry and wet environment for coatings on aluminum, noticing that the wear in a humid environment is less than in dry.

Hirpa G. Lemu (2013), also verified that in a humid environment the friction coefficient is lower than in the dry environment and affirms that the friction force increases as a function of time; Forlerer et al., (2000), performed friction wear tests on a block-on-ring machine with lubrication of mineral oil in a ZA27 alloy reinforced with Si, Cu precipitates and SiC particles of an average size of 5 microns. They verified that the most reinforced material is the most resistant to wear, and the non-reinforced friction coefficient is $\mu = 0{,}15$, while for reinforced materials is $\mu = 0{,}12$.

The word friction comes from the Latin "Fricare" which means friction or rubbing. It manifests itself as a gradual loss of kinetic energy when two bodies are in contact and in relative motion.

Defined as: the resistance force to the movement of a body, when it moves over another, being this force tangential to the interface and in the opposite direction to the displacement; causing energy consumption, accordingly, this force can be defined, based on the first thermodynamic law, as: the work done due to the friction force is equal to the sum of the increase in internal energy and the energy dissipated in the form of heat or temperature rise (ASM, ASM Handbook,1992, Vol. 18).

The French physicist Guillaume Amontons in 1699 quantitatively established the laws of friction. Later in 1748, Euler tried to explain the difference between the static and dynamic coefficient, but it was not until 1785 that José Marie Coulomb established the third fundamental law of this phenomenon.

It should be noted that the coefficient of friction for metals, as indicated by the 3rd law of friction, is independent of the sliding speed, but only up to 10 m/s, since after this value the coefficient of friction decreases as the velocity increases. (Hutchings. Tribology, 1992). Stembalski et Al. (2013), verified this principle in his study. Determination of the friction coefficient as a function of sliding speed and normal pressure for steel C45 and steel 40HM.

Asaduzzaman Ch. et Al. (2013) and Chowdhury M.A. *et al*., (2013), determined that although the normal load and the slip speed were varied, the force and the friction coefficient are stabilized after thirteen minutes of contact with the materials.

The static friction coefficient μs is obtained by placing a body on an inclined plane, as shown in Figure 1.

By increasing the angle of inclination φ, up to where the object begins to move; in this position, the static friction coefficient is determined, using the following equation (Bayer R. G., 1944):

$$\mu s = \frac{W \sin\varphi}{W \cos\varphi} = \operatorname{tg}\varphi \qquad (1)$$

ISSN-On line: 2444-4987

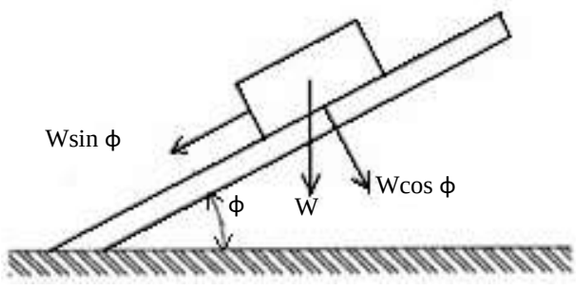

Figure 1 *Representation of friction angle*

Mechanical contact is one of the main phenomena that produce wear, generated by friction loads in systems that are exposed to high coefficients of friction; This principle is present in any system that is exposed to loads or dynamic movements, such as machinery and equipment used for construction, manufacturing processes, transportation, various services, and even our body is subjected to rotary movements that produce frictional forces. Frictional forces are an inevitable phenomenon that occurs whenever two surfaces interact, normally, controlled loads do not cause violent failures, but they generate functional consequences such as reduced efficiency, higher energy consumption, power losses and heat generation from the components, due to the increased coefficients of friction; this phenomenon becomes critical when there is no lubrication between the two surfaces in contact.

The measurement of frictional forces and the calculation of friction coefficients are frequently supported by the different tribometers. There are different types of tests to determine the coefficients of friction ranging from the inclined plane designed by Leonardo da Vinci; as well as the different standardized tests, such as those established by the American Standard Testing Materials (ASTM), or other organizations, such as the American National Standards Institute (ANSI) and the International Organization for Standardization (ISO) (Bayer RG, 1944).

To calculate the friction coefficient, the following equation is used:

$$\mu = \frac{f_r}{N} \qquad (2)$$

Where:

μ = Friction Coefficient

fr = Friction force
N = Applied normal force

Research methodology

The study consists of the preparation of three 5% Cr steel specimens, the machining conditions comply with the ASTM D2714 standard, the tribological system consists of the stationary block, made of the tested material (in our case 5% Cr steel), pressed at load P against the ring (in our case Steel D2), the equipment used for the test is the T-05 Block-on-Ring wear tester machine, which is shown graphically in Figure 2 a), and the illustration of the tribosystem in Figure 2 b). In this test, the ring is rotated with constant speed against the stationary block, and during the entire cycle is subjected to a constant load of 392N, and speeds of 0.18 m/sec for Sample 1, 0.36 m/sec for Sample 2 and 0.54 m/sec for Sample 3; taking contact force measurements by means of sensors connected to the CPU and measuring the wear track at the end of the test. The tests are performed in a tribometer to simulate wear in the absence of lubricant. The monitoring of the test lasts 800 seconds.

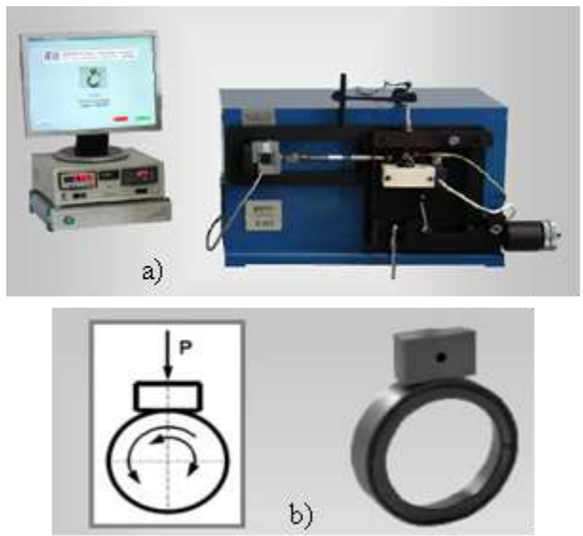

Figure 2 a) Machine T05 Block-on-ring b) Ilustration of tribosystem

Results

The 5% Cr steel samples have a hardness that varies in a range of 50-52 HRC; the chemical analysis of this material can be seen in Table 1, where it can be verified that, due to its low carbon content, it corresponds to a chromium-alloy steel.

ISSN-On line: 2444-4987

C	Si	Mn	Cr	Mo	V
0.55	0.15	0.60	5.00	0.80	0.15

Table 1 Chemistry composition of Steel 5%Cr

The wear in certain geometric contacts produces loss of material on one of the surfaces, initially the contact between the block and the disc is a line, but as it wears, the contact between both becomes an area where the track of wear in the block is observed as a rectangle, for our case of analysis we take the linear measurement of the width of the wear track considering four points to divide it, which are identified with the variables L1 to L4, we can see this distribution in Figure 3, and its dimensions are shown in Table 2, also indicating the average of each of the samples, which is 922,500 µm for Sample 1, 852,500 µm for Sample 2 and 772,500 µm for Sample 3.

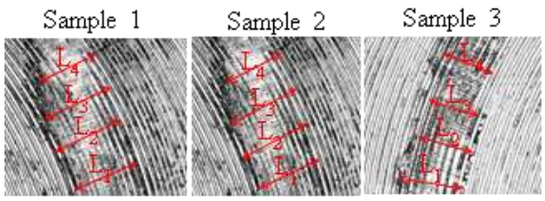

Figure 3 Identification of width on wear track for steel samples 5%Cr

Sample	L_1(µm)	L_2(µm)	L_3(µm)	L_4(µm)	L_{Prom} (µm)
1	970.000	1020.000	920.000	780.000	922.500
2	990.000	960.000	750.000	710.000	852.500
3	860.000	830.000	700.000	700.000	772.500

Table 2 Length of width on wear track for steel samples 5% Cr

The results obtained from the different tests are known as tribodata. In Graph 1, the behavior of the friction force as a function of time can be observed, indicating that the friction force is greater for Sample 1, which was tested with the lowest speed, these results coincide with the coefficient of friction, which is shown in Graph 2, which also shows that the coefficient of friction is greater for sample 1. For both cases of load and coefficient of friction, the test stabilizes and reaches its maximum values at approximately 350 sec.

In Graphic 3, it can be observed how the coefficient of friction has a linear behavior that decreases as a function of speed; the lowest coefficient of friction is 0.144 and corresponds to a speed of 0.54 m/sec.

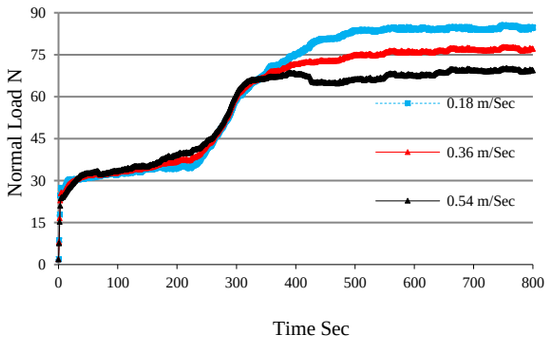

Graphic 1 Illustration of Friction load in function of time

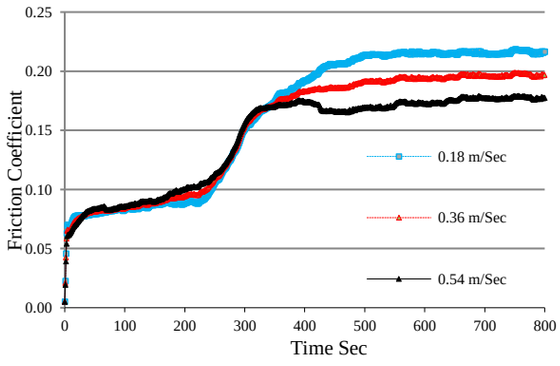

Graphic 2 Illustration of Friction Coefficient in function of time

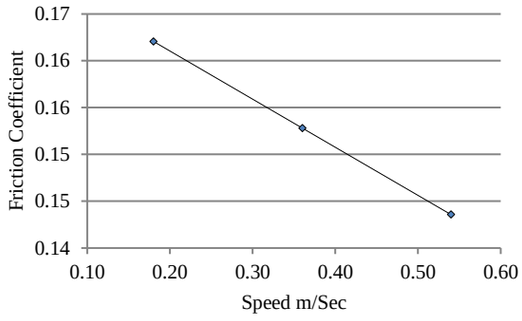

Graphic 3 Illustration of Friction Coefficient in function of speed

Conclusions

The width of the wear track is greater in Sample 1, which coincides with the greater friction force and the greater friction coefficient; thus, proving that wear is a function of speed; the higher the speed, the lower the friction coefficient and accordingly the lower the wear, as indicated by the 3rd law of friction for metals, according to Hutchings (1992).

This proves that the force and coefficient of friction stabilizes at approximately 13 minutes (800 seconds) according to the studies carried out by Asaduzzaman Ch. M. et al., (2013)

ISSN-On line: 2444-4987

It was shown that the friction coefficient values obtained in this study (μ=0.144), with speeds of 0.54 m/sec, are within the range of coefficients established by Forlerer et Al. (2000).

References

Asaduzzaman Ch. M., Muhammad N.D., Kumar R.B, Palash K.D, Golan M.M, Shahidul I.M, and Rashed M., (2013), Experimental Investigation on Friction and Wear of Stainless Steel 304 Sliding Against Different Pin Materials, World Applied Sciences Journal 22 (12): p.1702-1710. DOI:10.5829/idosi.wasj.2013.22.12.660

Asaduzzaman Ch. M., Muhammad N.D., Kumar R.B, Mostafizur R.M, Shahin M.M., Rashed M., and Bhumik S., (2013), Experimental investigation of friction coefficient and wear rate of different sliding pairs, World Applied Sciences Journal, 28 (5), p.608-619. DOI:10.5829/idosi.wasj.2013.28.05.1168

ASM, ASM Handbook (1992), Vol. 18, Friction, Lubrication, and Wear Technology, ASM International. USA.

Bayer R. G., (1944), Mechanical wear prediction an prevention, Edit Marcel Dekker.

Chowdhury M.A, Nuruzzaman D.M., Roy B.K., Samad S., Sarker R., Rezwan A.H.M; (2013), Experimental investigation of friction coefficient and wear rate of composite materials sliding against smooth and rough mild steel counterfaces; Tribology in industry; Vol.35 No.4, p.286-296. www.tribology.rs/journals/2013/2013-4/5.pdf

Deuis R.L, Subramanian C., and Yellup J.M.,(1998), Three-body abrasive wear of composite coatings in dry and wet environments, Wear 214, p.112-130. DOI:10.1016/S0043-1648(97)00197-X

Forlerer E., Auras R., Montero R., Calderon S. y Schvezov C.E., (2000), Desgaste por fricción en la aleación de Zn-Al:ZA27 y en un compuesto de ZA27 reforzado con Si y CSi., p.451-458.

Hirpa G.L, Trzepiecinski T., (2013) Numerical and experimental study of Friction Behavior in Bending Under Tension Test, Journal of Mechanical Engineering, 59 (1), p.41-49. DOI:10.5545/sv-jme.2012.383

Hutchings.Tribology: (1992), Friction and wear of engineering materials, Edit. Great Britain.

Stembalski M., Pres´ P., Skoczyeski W.,(2013), Determination of the friction coefficient as a function of sliding speed and normal pressure for C45 and steel 40HM, Archives of civil and mechanical engineering, 13, p.444-448. DOI:10.1016/j.acme.2013.04.010

Wirojanupatump S. (1999), A direct comparision of wet and dry conditions with the rubber and steel, Wear Vol.223-235, p.655-665.

ISSN-On line: 2444-4987

Article **Journal of Research and Development**
June 2022, Vol.8 No.21 6-13

Design process for dual coplanar waveguide directional couplers for power transmission

Proceso de diseño de acopladores direccionales con guía de onda coplanar diferencial para transmisión de potencia

CASTAÑEDA-IBARRA, Víctor R.†, CISNEROS-SINENCIO, Luis F.*, GARCÍA-VITE, Pedro M. and CASTILLO-GUTIÉRREZ, Rafael

Tecnológico Nacional de México, Instituto Tecnológico de Ciudad Madero, Mexico.

ID 1st Author: *Víctor Rodrígo, Castañeda-Ibarra* / **ORC ID:** 0000-0003-3863-0553, **CVU CONACYT ID:** 1083997

ID 1st Co-author: *Luis Fortino, Cisneros-Sinencio* / **CVU CONACYT ID:** 102695

ID 2nd Co-author: *Pedro Martín, García-Vite* / **ORC ID:** 0000-0001-6019-7958, **CVU CONACYT ID:** 227310

ID 3rd Co-author: *Rafael, Castillo-Gutiérrez* / **ORC ID:** 0000-0001-8599-892X, **CVU CONACYT ID:** 63299

DOI: 10.35429/JRD.2022.21.8.6.13 Received: January 20, 2022; Accepted: May 30, 2022

Abstract

In this paper, a design process for power directional couplers using dual conductor-backed coplanar waveguides (CBCPW), is presented. The proposed methodology is applied to the design of a 50 Ω impedance coupler with 10 dB coupling factor for a central frequency of 2.5 GHz. The resulting coupler is validated through simulation by obtaining its dispersion parameters using ANSYS High Frequency Structure Simulator (HFSS). From the analysis of the return loss, insertion loss and coupling factor, in a range of 1 to 4 GHz, it was found that the coupling factor complies with the design specification for frequencies from 2 to 3 GHz, with insertion losses between -1 and -2 dB around the center frequency and return losses of -15 dB.

Methodology, directional coupling, coplanar waveguide, dispersion parameters

Resumen

En este trabajo se propone un proceso de diseño para acopladores direccionales de potencia construidos con guías de onda coplanares con conductor de respaldo (CBCPW) duales. Esta propuesta se aplicará en el diseño de un acoplador con impedancia de 50 Ω y un factor de acoplamiento de 10 dB para una frecuencia central de 2.5 GHz. El proceso de diseño será validado a través de sus parámetros de dispersión obtenidos mediante el Simulador de Estructuras en Alta Frecuencia de Ansys (HFSS). De acuerdo al análisis de las gráficas de pérdidas de retorno, de pérdidas de inserción y de factor de acoplamiento, en un rango de 1 a 4 GHz, se comprobó que el factor de acoplamiento cumple con la especificación de diseño para frecuencias de 2 a 3 GHz, con pérdidas de inserción entre los -1 y -2 dB alrededor de la frecuencia central y pérdidas de retorno de -15 dB.

Metodología, acoplador direccional, guía de onda coplanar, parámetros de dispersión

Citation: CASTAÑEDA-IBARRA, Víctor R., CISNEROS-SINENCIO, Luis F., GARCÍA-VITE, Pedro M. and CASTILLO-GUTIÉRREZ, Rafael. Design of dual coplanar waveguide directional couplers for power transmisión. Journal of Research and Development. 2022. 8-21:6-13.

* Author's Correspondence (E-mail: fortino.cs@cdmadero.tecnm.mx)
† Researcher contributing as first author.

Introduction

Directional couplers are four- or three-port linear passive devices used to couple power from a transmission line to a coupled port (Avionics Department, 2013). These circuits are constructed using two transmission lines that are placed close enough to each other so that some of the power travelling on one line can be transmitted to the other line with a known attenuation; this phenomenon is known as coupling (Simons 2001). The coupled output of this device is used to obtain information from a signal without interrupting the power flow in the system, with small insertion loss due to coupling. Figure 1 shows the structure of a directional coupler along with the power flow through its ports; because they are linear devices, the distribution of its ports is arbitrary, so any port can serve as an input.

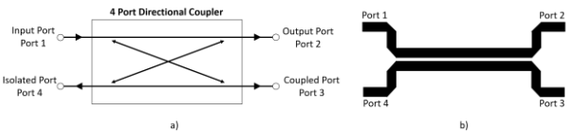

Figure 1 Directional Coupler a) Schematic and b) Structure of a directional microstrip coupler

The structure of such circuits can consist of different types of transmission lines such as: strip lines, microstrip lines and waveguides, each with different coupling capabilities (Roshani, et al., 2022). The field of application of each of these options will depend on their range of coupling values. Very weak coupling values relate to microwave power monitoring applications; for example, for sampling incident and reflected waves in reflectometers, a fundamental part of vector or scalar network analysers (Mousavi, et al., 2015). Other applications of directional couplers relate to signal distribution in antenna networks, balanced circuits and mixing applications (Liang, et al., 2007) (Shi, et al., 2008) (Shi, et al., 2010) (Chen & Xue, 2013) (Liu, et al., 2014) (Yu & Yang, 2022) (Zhao, et al., 2022).

The length of the coupled lines of a directional coupler must measure at least one quarter of the wavelength. When this condition is met, the coupling factor (k) reaches its maximum value, optimising the power transfer from the input port to the coupled port. This factor can be defined as the inverse of the fraction of voltage transferred.

Depending on the application, this factor can take different values, typically between 3 and 40 dB. Other important parameters in coupler design are the transmission factor, directivity factor and isolation factor.

- The transmission factor represents the power that is transferred from port 1 to port 2 through the main line of the structure, its ideal value expressed in dB is equal to $20\log\left|\sqrt{1-1/C^2}\right|$ dB, with a typical value of 0.5 dB.

- The directivity factor describes the magnitude of the unwanted coupling between port 1 and port 4 compared to the coupling at port 3; the higher this value, the higher the directivity of the coupler. Its typical value is 40 dB.

- The isolation factor describes how much of the power applied to port 1 is directed to port 4. Ideally this value is very high, tending towards infinity, however, in real systems, its magnitude is around 40 dB.

Characteristics of the coupled lines

Any pair of coupled transmission lines can be described as a four-port configuration, where one of the lines (or both depending on the transmission mode) carries a signal that is induced into the adjacent line, generating charges and currents on the adjacent line. Since the field pattern (mode) on the pair of lines is the result of the linear superposition of each of the individual field patterns; when they travel in the same direction it is called an even mode; and when both waves travel in the opposite direction it is called an odd mode (Edwards, 2016). Figure 2 shows the directions of both the electric field and the magnetic field for each of the modes in a coplanar line structure. It can be deduced that the behaviour of a coupled structure is the result of the superposition of the effects of both modes. Due to the difference in the distribution of fields in each mode, two different characteristic impedances are defined; one corresponding to the even mode (Z_{0e}) and the other for the odd mode (Z_{0o}).

ISSN-On line: 2444-4987

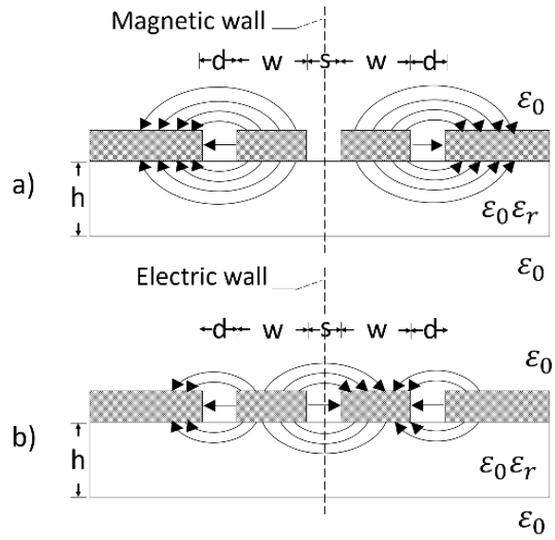

Figure 2 Direction of magnetic and electric fields in coupled lines a) Even mode and b) Odd mode

The design process of a directional coupler consists of determining the physical dimensions of a coupled line structure. The calculation of these parameters is derived from the odd and even mode impedances Z_{0e} and Z_{0o} impedances (Edwards, 2016). The ratio of these impedances to *k* and Z_{S0} se describe en (Wadell, 1991). is described in (Wadell, 1991). By solving these equations, it is possible to plot the relationship between the line impedances and their coupling factor for Z_{0s} = 50 Ω. This relationship is shown in the graph in Figure 3, where it can be seen that the closer the two impedance values, odd and even, at Z_{0s}, the coupling between lines decreases, minimising the power transfer from one line to the other. Conversely, if the difference between these values increases, so does the coupling between lines.

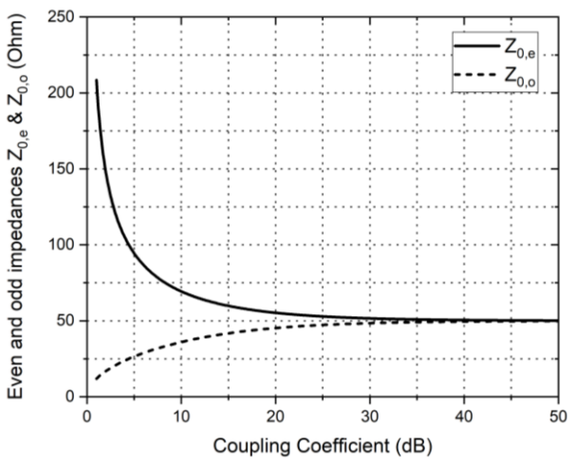

Figure 3 Even and odd mode impedance Z_{0e} and Z_{0o} (Ω) with respect to coupling coefficient *k* (dB)

The level of coupling between the two lines also depends on the length of the coupled structure, finding its maximum when the length of the line is equal to one quarter of the wavelength ($\lambda_g/4$), i.e., when the electrical length θ is equal to π/2.

Structures of a CBCPW

A coplanar waveguide (CPW) consists of a conductor line mounted on a dielectric that has a return conductor on each side of the line, both located in the same plane as the centre conductor (He, et al., 2022). A coplanar wave with backup conductor (CBCPW) is a coplanar waveguide to which an additional ground conductor is added in a second plane located on the other side of the substrate. Both waveguides share characteristics such as ease of being connected in series and shunt, low radiation and low dispersion, so they are widely used in power splitters, mixers, band-pass filters, Lange couplers, high directivity couplers and switched transmission lines (Watson & Gupta, 1997) (Kim, et al., 2002) (Tessmann, 2006) (Chen, et al., 2010) (Wane, et al., 2015) (Xiao, et al., 2016) (Du, et al., 2022).

The characteristics of a CBCPW are defined by its dimensions, being: the width of its central conductor (*2a*), the spacing between the two adjacent ground planes (*2b*), as well as the height of the substrate (*h*). Figure 4 shows the CBCPW structure with its different dimensions.

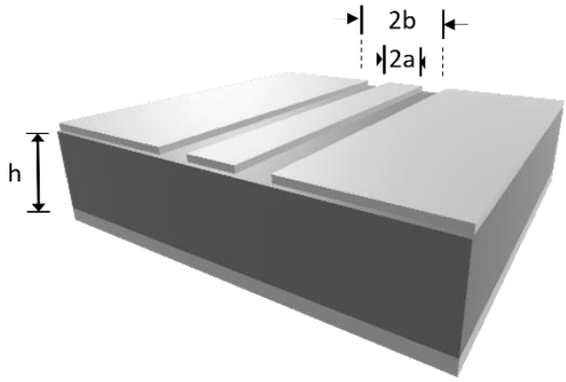

Figure 4 Cross-sectional dimensions of a coplanar waveguide with back-up conductor (*a*, *b*, *h*).

In the case of a dual CBCPW, as shown in Figure 5, there are two centre conductors. In this case, the line dimensions are: the distance between the two signal lines (*s*), the spacing to adjacent ground planes (*d*), the width of the centre conductors (*w*) and the height of the substrate (*h*).

ISSN-On line: 2444-4987

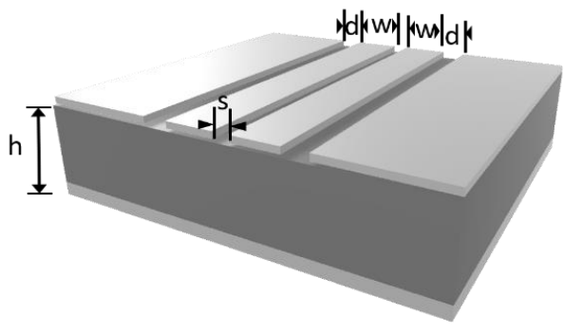

Figure 5 Cross-sectional dimensions of a dual coplanar waveguide with back-up conductor (*d*, *w*, *s*, *h*)

Characteristic impedance of a CBCPW

In (Wadell, 1991) and (Simons, 2001) the equations relating each of the dimensions of a coplanar waveguide to its impedances are described for both a CBCPW and a dual CBCPW structure. With the help of Octave mathematical software, these equations were solved to relate different line parameters. The graph in Figure 6 shows the relationship between the coupling coefficient *k* and the factor *s/(s+2w)* for different values of *[(s/2)+w]/h* with Z_{0s}=50 Ω, *h*=1.6, ε_r=4.0 and *d*=s.

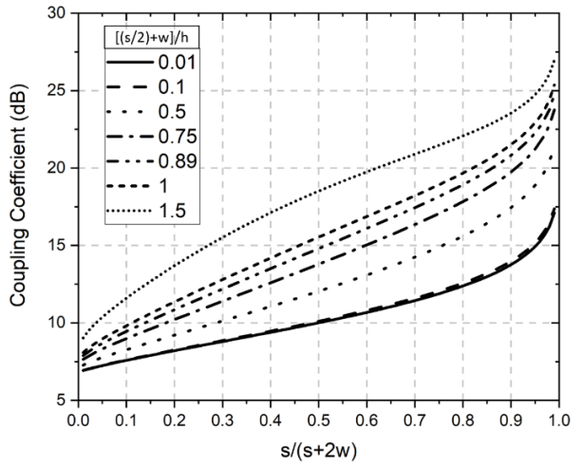

Figure 6 Coupling coefficient *k* (dB) with respect to different values of *s/(s+2w)* for different values of *[(s/2)+w]/h* with Z_{s0}=50Ω, *h*=1.6, ε_r=4.0 and with *d*=s.

The graph in Figure 7 shows the relationship between $Z_{0,e}$ and $Z_{0,o}$ for different values of *s/h* and *w/h* with *d*=*s*.

Both graphs will be useful in determining the dimensions of the coupler as a function of its k-factor and its characteristic impedance.

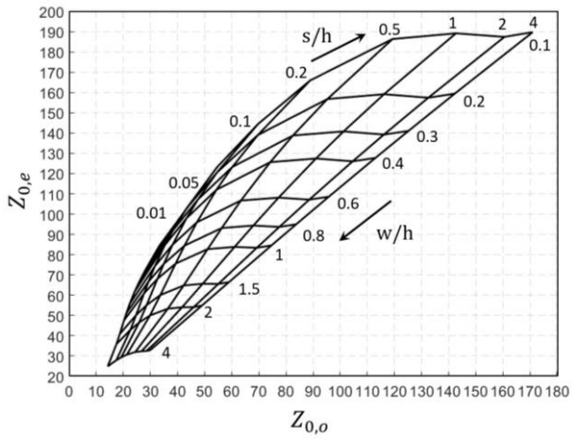

Figure 7 Odd and even mode impedances $Z_{0,e}$ and $Z_{0,e}$ with respect to different ratios of *s/h* and *w/h* with *d*=*s*.

Directional coupler design

Figure 8 shows the structure of the directional coupler of interest, where two different sections can be identified. The first section is characterised by two parallel conductor lines (constant s); for this section the design equations for a dual CBCPW will be used. In the second section, s varies continuously, so the previous equations are no longer valid; for this section, the design equations for a simple CBCPW are used. Thus, considering the coupler as three different waveguides connected in series, it is possible to ensure an impedance of 50 Ω throughout the device.

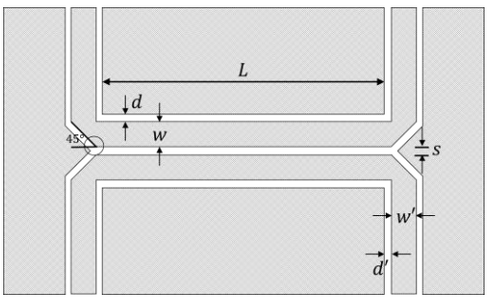

Figure 8 Physical dimensions involved in the electrical characteristics of a directional coupler using a CBCPW structure

The calculations for the construction of a Dual CBCPW with a characteristic impedance of 50 Ω and a coupling factor of 10 dB are presented below. From the graph in Figure 3 we get $Z_{0,e} = 69.269\ \Omega$ and $Z_{0,o} = 36.185\ \Omega$. In turn, with the help of graphs in Figures 6 and 7, it is found that these impedances can be achieved with a ratio s/h= 0.18 and w/h=1.18. Taking h=1.6 and $\varepsilon_r = 4.0$, corresponding to the substrate of a commercial PCB manufactured with FR-4, we have.

ISSN-On line: 2444-4987

h=1.6 s=0.3 d=0.3 w=1.91 ε_r=4.0

Once the transverse parameters have been obtained, it is necessary to calculate the length of the coupled section. For this, it is necessary to calculate the effective even and odd mode permittivities $\varepsilon_{eff,e}$ y $\varepsilon_{eff,o}$, so that:

$$r = \frac{s}{s+2w} = 0.0728 \quad (1)$$

$$k_1 = \frac{s+2w}{s+2w+2d} = 0.8729 \quad (2)$$

$$\beta_1 = \left[\frac{(1-r^2)}{(1-{k_1}^2 r^2)}\right]^{1/2} = 0.9994 \quad (3)$$

$$\Lambda = \frac{\sinh\left[\frac{\pi(\frac{s}{2}+w+d)}{2h}\right]^2}{2} = 12.6150 \quad (4)$$

$$\Lambda' = \frac{\cosh\left[\frac{\pi(\frac{s}{2}+w+d)}{2h}\right]^2}{2.0} = 13.1150 \quad (5)$$

$$t_c = \sinh\left[\frac{\pi(\frac{s}{2}+w)}{2\,h}\right]^2 - \Lambda = 1.1644 \quad (6)$$

$$t'_c = \sinh\left[\frac{\pi(\frac{s}{2}+w)}{2h}\right]^2 - \Lambda' + 1.0 = 1.6644 \quad (7)$$

$$t_B = \sinh\left(\frac{\pi\, s}{4h}\right)^2 - \Lambda = -12.5932 \quad (8)$$

$$t'_B = \sinh\left[\frac{\pi\, s}{4h}\right]^2 - \Lambda' + 1.0 = -11.9660 \quad (9)$$

$$k_o = \Lambda \frac{-\sqrt{\Lambda^2-{t_c}^2}+\sqrt{\Lambda^2-{t_B}^2}}{t_B\sqrt{\Lambda^2-{t_c}^2}+t_c\sqrt{\Lambda^2-{t_B}^2}} = 0.9477 \quad (10)$$

$$k_e = \Lambda' \frac{-\sqrt{\Lambda'^2-{t'_c}^2}+\sqrt{\Lambda'^2-{t'_B}^2}}{t'_B\sqrt{\Lambda'^2-{t'_c}^2}+t'_c\sqrt{\Lambda'^2-{t'_B}^2}} = 0.6829 \quad (11)$$

$$\varepsilon_{eff,o} = \frac{2\varepsilon_r\frac{K(k_o)}{K'(k_o)}+\frac{K(\beta_1)}{K'(\beta_1)}}{2\frac{K(k_o)}{K'(k_o)}+\frac{K(\beta_1)}{K'(\beta_1)}} = 2.5342 \quad (12)$$

$$\varepsilon_{eff,e} = \frac{2\varepsilon_r\frac{K(k_e)}{K'(k_e)}+\frac{K(\beta_1 k_1)}{K'(\beta_1 k_1)}}{2.0\frac{K(k_e)}{K'(k_e)}+\frac{K(\beta_1 k_1)}{K'(\beta_1 k_1)}} = 2.7739 \quad (13)$$

Because the two permittivities are different, to find the wavelength it is necessary to calculate the average of the two permittivities.

$$\varepsilon_{eff,avg} = \frac{\varepsilon_{eff,e}+\varepsilon_{eff,o}}{2} = \frac{2.7739+2.5342}{2} = 2.6540 \quad (14)$$

Thus, the average wavelength is:

$$\lambda_g = \frac{c}{f\sqrt{\varepsilon_{eff,avg}}} = \frac{3\cdot 10^{11}}{2.5^9\sqrt{2.654}} = 73.65\ mm \quad (15)$$

Therefore, the length of the coupler should be:

$$L = \lambda_g/4 = 18.414\ mm \quad (16)$$

Finally, the dimensions of the lines going to each of the ports are calculated using the equations for a simple CBCPW manufactured in the same commercial process with FR-4, thus $Z_{0s} = 50\ \Omega$, a=1.91, $h = 1.6$ y $\varepsilon_r = 4.0$. The following calculations are then performed:

$$k = \frac{a}{b} = (1.91)/(2.64) = 0.7235 \quad (17)$$

$$k_1 = \frac{\tanh\left(\frac{\pi a}{4h}\right)}{\tanh\left(\frac{\pi b}{4h}\right)} = 0.8529 \quad (18)$$

$$k' = \sqrt{1.0-k^2} = 0.6903 \quad (19)$$

$$k'_1 = \sqrt{1.0-{k_1}^2} = 0.5220 \quad (20)$$

ISSN-On line: 2444-4987

$$\varepsilon_{eff} = \frac{1.0 + \varepsilon_r \frac{K(k')}{K(k)} \frac{K(k_1)}{K(k'_1)}}{1.0 + \frac{K(k')}{K(k)} \frac{K(k_1)}{K(k'_1)}} = 2.66 \quad (21)$$

$$Z_0 = \frac{60\pi}{\sqrt{\varepsilon_{eff}}} \left[\frac{1.0}{\frac{K(k)}{K(k')} + \frac{K(k_1)}{K(k'_1)}} \right] = 50.087\ \Omega \quad (22)$$

The dimensions of the coupled section are shown in Table 1, while for the single waveguide section they are shown in Table 2.

Parameter	
k	3.188 (10 dB)
Z_{S0}	50 Ω
ε_r	4.0
t	0.035 mm
d	0.3 mm
w	1.91 mm
s	0.3 mm
h	1.6 mm
L	18.414 mm

Table 1 Physical and electrical parameters of the CBCPW Dual (coupled section)

Parameter	
Z_{S0}	50 Ω
ε_r	4.0
t	0.035 mm
a	1.91 mm
b	2.64 m
h	0 mm

Table 2 Physical and electrical parameters of the single CBCPW

Results

To validate the design of the directional coupler, its dispersion parameters obtained by simulation using Ansys High Frequency Structure Simulator (HFSS) will be analysed.

The graph in Figure 9 shows the return loss at ports 1, 2 and 3, which correspond to the input port, direct output port and the coupled port respectively. The graph shows that the return loss at all ports remains below -10 dB over the entire frequency spectrum and close to -15 dB around the frequency of interest. Overall, a low level of return loss is shown, thus demonstrating that the design specifications are met.

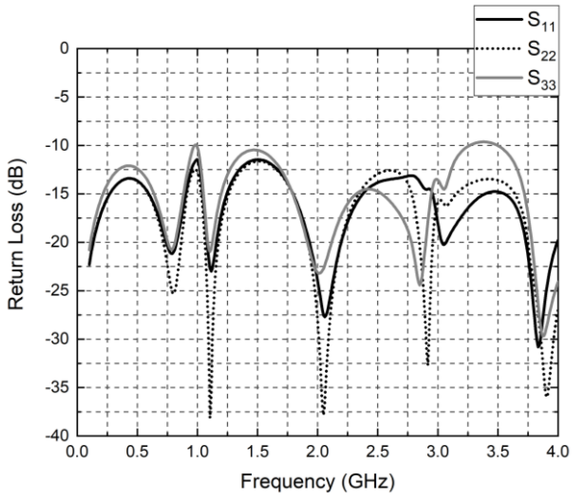

Figure 9 Return loss (dB), parameters S_{11}, S_{22}, S_{33} in a frequency range of 1 to 4 GHz

The graph in Figure 10 shows the insertion losses corresponding to parameter S_{12}, the coupling level in the parameter S_{13} and the isolation level on port 4 in parameter S_{14}. The graph shows that this parameter is above -5 dB over the entire frequency range sampled and between -1 and -2 dB around the frequency of interest, demonstrating that the coupler has low transmission losses from the input port to the direct port.

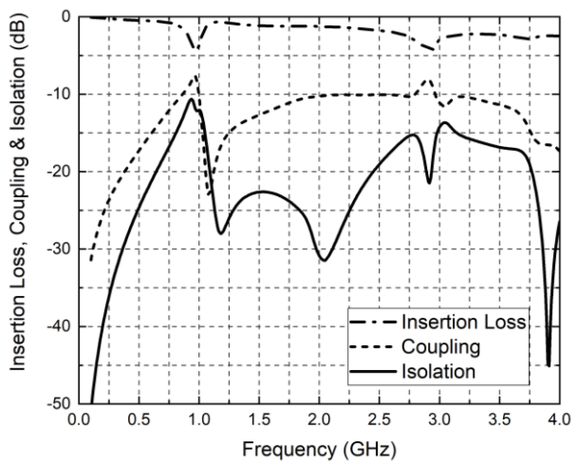

Figure 10 Insertion loss, coupling and isolation factor (dB), in a frequency range from 1 to 4 GHz

On the other hand, the blue curve shows how the coupling factor (coupling) remains at -10 dB for frequency values between 2 and 2.75 GHz. In turn, the isolation factor (isolation) is maintained at values below -15 dB in almost the entire frequency spectrum, with a minimum of -37 dB at 2 GHz; in general, good levels of both coupling and isolation are observed for the entire sampled range.

ISSN-On line: 2444-4987

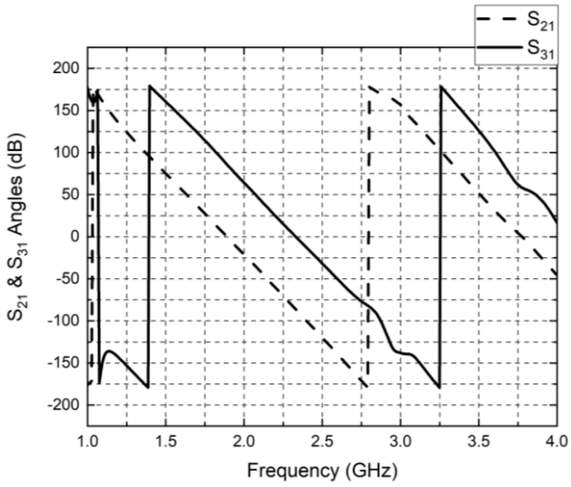

Figure 11 Angles of S_{12} y S_{13} expressed in degrees over a frequency range of 1 to 4 GHz

Finally, the angles of the parameters are S_{12} and S_{13} shown in degrees. In a directional coupler, there must be a phase shift of 90° between the output signal at port 2 and the coupled signal at port 3. From the graph in Figure 12, a phase shift close to 90° is observed between the two signals, a condition that is met for a range of 1.4 to 2.75 GHz.

Acknowledgements

The authors would like to thank the Tecnológico Nacional de México/Instituto Tecnológico de Ciudad Madero and the Consejo Nacional de Ciencia y Tecnología CONACyT for funding the development of this project.

Conclusions

From the analysis of the results obtained by simulation, a coupling factor of -10 dB is observed in the frequency range from 1.75 to 2.75 GHz. Also, it is observed that in the same range a good level of isolation is achieved at the frequency of interest, which remains below -15 dB in almost the entire sampled spectrum and at a value of -18 dB at the centre frequency. The return loss remains below -10 dB throughout the range, i.e. there are low levels of return loss. Furthermore, it can be observed that the power transferred to the direct port decreases by -1.8 dB with respect to the incident power and that the angle between the two signals is 4° above 90°, i.e. 4.4% of the ideal value.

This shows that the coupler complies with the specifications by presenting low insertion and return loss, a good level of coupling at the centre frequency (2.5 GHz) and a good level of isolation of less than -15 dB.

References

Avionics Department (2013). Power Dividers and Directional Couplers, *Electronic Warfare and Radar Systems Engineering Handbook*, Technical Communication Office, VI, 4, 276–281.

Chen, S. & Xue, Q. (2013). Compact triple-transistor Doherty amplifier designs: differential/power combining, *IEEE transactions on microwave theory and techniques*, 61(5), 1957–1963. https://doi.org/10.1109/TMTT.2013.2253794

Chen, X. P., Wu, K., Han, L. & He, F. (2010). Low-cost high gain planar antenna array for 60-GHz band applications, *IEEE Transactions on Antennas and Propagation*, 58(6), 2126–2129. https://doi.org/10.1109/TAP.2010.2046861

Du, C., Yang, Z., Jin, G., & Zhong, S. (2022). Design of a co-planar waveguide-fed flexible ultra-wideband-multiple-input multiple-output antenna with dual band-notched characteristics for wireless body area network. *International Journal of RF and Microwave Computer-Aided*

Edwards, T. C. (2016). Parallel-coupled Microstrip Lines, *Foundations for microstrip circuit design*, 4th ed. John Wiley & Sons, 10, 10.1-10.5, 268–304. https://doi.org/10.1002/9781118936160.ch10

He, Q., OuYang, P., Gao, H., Li, Y., Wang, Y., Chen, Y., ... & Wei, L. F. (2022). Low-loss superconducting aluminum microwave coplanar waveguide resonators on sapphires for the qubit readouts. *Superconductor Science and Technology*, 35, 6. http://dx.doi.org/10.1088/1361-6668/ac6a1d

Kim, D., Choi, H. Y., Allen, M. G., Kenney, J. S. & Kiesling, D. (2002). A wide bandwidth monolithic BST reflection-type phase shifter using a coplanar waveguide Lange coupler, *2002 IEEE MTT-S International Microwave Symposium Digest (Cat. No. 02CH37278)*, 3, 531–533.

https://doi.org/10.1109/MWSYM.2002.1012133

Liang, K. H., Chang, H. Y. & Chan, Y. J. (2007). A 0.5-7.5 GHz Ultra Low Voltage Low-Power Mixer Using Bulk-Injection Method by 0.18-um CMOS Technology, *IEEE Microwave and Wireless Components Letters*, 17(7), 531–533. https://doi.org/10.1109/LMWC.2007.899319

Liu, J. Y. C., Chen, J. S., Hsia, C., Yin, P. Y. & Lu, C. W. (2014). A wideband inductorless single-to-differential LNA in 0.18um CMOS technology for digital TV receivers, *IEEE microwave and wireless components letters*, 24(7), 472–474. https://doi.org/10.1109/LMWC.2014.2316495

Mousavi, S. M., Mirtaheri, S. A., Khosravani-Moghaddam, M. A., Habibi, B. & Meiguni, J. S. (2015). Design, fabrication and test of a broadband high, directivity directional coupler. *IEEE 23rd Iranian Conference on Electrical Engineering*, 168–170. http://dx.doi.org/10.1109/IranianCEE.2015.7146203

Roshani, S., Azizian, J., Roshani, S., Jamshidi, M. B., & Parandin, F. (2022). Design of a miniaturized branch line microstrip coupler with a simple structure using artificial neural network. *Frequenz*, 76(5-6). http://dx.doi.org/10.1515/freq-2021-0172

Shi, J. & Xue, Q. (2010). Balanced band pass filters using center-loaded half-wavelength resonators, *IEEE transactions on microwave theory and techniques*, 58(4), 970–977. https://doi.org/10.1109/TMTT.2010.2042839

Shi, J., Chen, J. X. & Xue, Q. (2008). A novel differential bandpass filter based on double-sided parallel-strip line dual-mode resonator, *Microwave and Optical Technology Letters*, 50(7), 1733–1735. https://doi.org/10.1002/mop.23493

Simons, R. N. (2001). Directional Couplers, Hybrids, and Magic T's *Coplanar Waveguide Circuits, Components, and Systems*, John Wiley & Sons,Inc. 165, 11, 11.2, 346–352. https://doi.org/10.1002/0471224758.ch11

Simons, R. N. (2001). Microshield Lines and Coupled Coplanar Waveguide, *Coplanar Waveguide Circuits, Components, and Systems*, Vol. 165. John Wiley & Sons, Inc 7, 7.4, 190–193. https://doi.org/10.1002/0471224758.ch7

Tessmann, A., Kuri, M., Riessle, M., Massler, H., Zink, M., Reinert, W. & Leuther, A. (2006). A compact W-band dual-channel receiver module *IEEE MTT-S International Microwave Symposium Digest*, 85–88. IEEE. https://doi.org/10.1109/MWSYM.2006.249934

Wadell, B. C. (1991). Coupled Lines. *Transmission line design handbook*, Artech House Microwave Library, IV, 4.4.3, 196–198.

Wane, S., Leyssenne, L., Tesson, O., Doussin, O., Bajon, D., Lesénéchal, D. & Erdem, A. (2015). Design of Lange Couplers with local ground references using SiGe BiCMOS technology for mm-Wave applications, 2015 *IEEE Radio Frequency Integrated Circuits Symposium (RFIC)*, 17(7), 351–354. https://doi.org/10.1109/RFIC.2015.7337777

Watson, P. M. & Gupta, K. C. (1997). Design and optimization of CPW circuits using EM-ANN models for CPW components, IEEE *Transactions on Microwave Theory and Techniques*, 45(12), 2515–2523. https://doi.org/10.1109/22.643868

Xiao, J. K., Zhu, M., Ma, J. G. & Hong, J. S. (2016). Conductor-backed CPW bandpass filters with electromagnetic couplings, *IEEE Microwave and Wireless Components Letters*, 26(6), 401–403. https://doi.org/10.1109/LMWC.2016.2562641

Yu, F., & Yang, X. X. (2022). Progress of Rectenna Arrays for Microwave Power Transmission Systems. *Advances in Astronautics Science and Technology*, 1-10. http://dx.doi.org/10.1007/s42423-022-00100-0

Zhao, Y., Dong, J., Yin, F., Fang, X., & Xiao, K. (2022). Broadband Coplanar Waveguide to Air-Filled Rectangular Waveguide Transition. *Electronics*, 11(7), 1057. http://dx.doi.org/10.3390/electronics11071057

ISSN-On line: 2444-4987

Article **Journal of Research and Development**
June 2022, Vol.8 No.21 14-20

Assessment of an organic Rankine cycle and a Kalina cycle for a single source of low-enthalpy geothermal heat

Evaluación de un ciclo Rankine orgánico y un ciclo Kalina para una misma fuente de calor geotérmica de baja entalpía

VERA-ROMERO, Iván†*, MARTÍNEZ-REYES, José and MÉNDEZ-ÁBREGO, V. Manuel

Universidad de la Ciénega del Estado de Michoacán de Ocampo, Mexico.

ID 1st Author: *Iván, Vera-Romero* / **ORC ID:** 0000-0003-1771-6630, **CVU CONACYT ID:** 102272

ID 1st Co-author: *José, Martínez-Reyes* / **ORC ID:** 0000-0001-6601-1851, **CVU CONACYT ID:** 232124

ID 2nd Co-author: *V. Manuel, Méndez-Ábrego* / **ORC ID:** 0000-0003-3409-8619, **CVU CONACYT ID:** 596022

DOI: 10.35429/JRD.2022.21.8.14.20 Received: January 25, 2022; Accepted: May 30, 2022

Abstract

This article shows the simulation results of an organic Rankine cycle (ORC) operating with the R134a working fluid and a Kalina Cycle operating with the ammonia-water mixture in order to compare the results and detect the better performing cycle. The working conditions were attained through a field visit to the town of Los Negritos, Michoacán, where it was determined that it is a superficial low-enthalpy source. To conduct the simulations, the Software Engineering Equation Solver (EES^{TM}) was employed. In the ORC, a net electric power output of 10.97 kWe was obtained with 4.58% cycle efficiency, while with the Kalina cycle, a net power output of 5.53 kWe was obtained along with an overall efficiency of 6.61%.

Energy evaluation, Geothermal energy, Thermodynamic cycles

Resumen

El siguiente trabajo muestra los resultados de la simulación de un Ciclo Rankiene Orgánico (ORC) operando con el fluido de trabajo R134a y un Ciclo Kalina operando con la mezcla amoniaco-agua, con la finalidad de comparar los resultados y detectar el ciclo con mejor desempeño. Las condiciones de trabajo se obtuvieron a través de una visita de campo a la localidad Los Negritos, Michoacán, donde se determinó que se trata de una fuente de baja entalpía superficial. Para realizar las simulaciones se empleó el Software Engineering Equation Solver (EES^{TM}). En el ORC se obtuvo una potencia eléctrica neta de salida de 10.97kWe con una eficiencia del ciclo de 4.58%, mientras que con el ciclo Kalina se obtuvo una potencia neta de salida de 5.53kWe y una eficiencia global de 6.61%.

Evaluación energética, Energía Geotérmica, Ciclos termodinámicos

Citation: VERA-ROMERO, Iván, MARTÍNEZ-REYES, José and MÉNDEZ-ÁBREGO, V. Manuel. Assessment of an organic Rankine cycle and a Kalina cycle for a single source of low-enthalpy geothermal heat. Journal of Research and Development. 2022. 8-21:14-20.

* Author's Correspondence (E-mail: ivera@ucemich.edu.mx)
† Researcher contributing as first author.

Introduction

Mexico's energy production is primarily based on fossil fuels (86.90%), while renewable resources contribute 11.25%, as seen in Figure 1 (SENER, 2021). However, conducting energy power studies is of vital importance- especially of the energy sources that can be exploited in a reliable and safe way- in order to diversify the national energy matrix and simultaneously focus on distributed, non-centralized generation (Abrigo, 2022). Accordingly, geothermal energy is a viable alternative, given that previously tested technology can be applied (Fridleifsson, 2001; Noorollahi, Shabbir, Siddiqi, Ilyashenko, & Ahmadi, 2019; Palomo-Torrejón, Colmenar-Santos, Rosales-Asensio, & Mur-Pérez, 2021). Renewable energies in Mexico are diversified as seen in Figure 2, where the most exploited or used is biomass (6.34%), firewood (4.87%), followed by geothermal (1.65%), and then cane bagasse (1.47%).

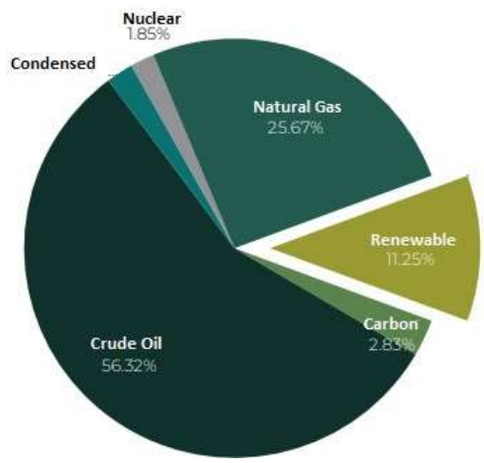

Figure 1 Production of primary energy in Mexico
Source: (SENER, 2021)

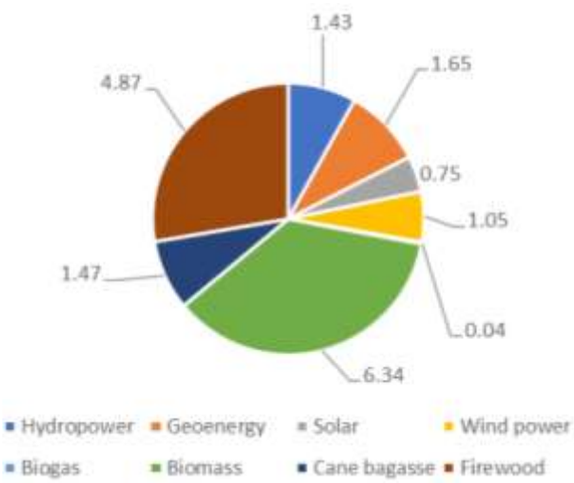

Figure 2 Contribution of renewable energies
Source: *(SIE, 2022)*

By 2020, Mexico was in sixth place worldwide in regard to the use of its geothermal energy resources (Huttrer, 2020). Currently, there are plants established in Cierro Prieto, Los Azufres, Los Humeros, Tres Vírgenes, and Domo San Pedro (Villeda, Zúñiga, & Flores, 2021). The state of Michoacán is located on the Trans-Mexican Volcanic Belt (Gómez-Tuena, Orozco-Esquivel, & Ferrari, 2005), where in addition to there being manifestations of geothermal energy in the Los Azufres zone, sites in the Ciénega de Chapala Region have been studied and identified, including Ixtlán, Pajacuarán, and Los Negritos (Martínez R. J., 2014).

Accordingly, the Los Negritos zone—located in the Villamar municipality in the state of Michoacán—has been selected to conduct a feasibility study on the generation of electric energy, taking advantage of the zone's superficial geothermal resource (Molés, Navarro-Esbrí, Peris, Mota-Babiloni, & Kontomaris, 2015). To this end, this article analyzes an organic Rankine cycle operating with a R134a working fluid (Vera-Romero, Corona-Ruíz, Reyes, Nava, & Murillo, 2018) and also a Kalina cycle, which is still a steam cycle, but it operates with a binary mixture of ammonia and water (Madhawa Hettiarachchi, Golubovic, Worek, & Ikegami, 2007). The results will be compared to detect the benefits of one cycle in contrast with the other, both for each set of equipment and in general by measuring the net power output and the cycle's overall efficiency.

Metodology

To determine the cycles' operating conditions, a field visit was made to the Los Negritos area, located 10 km east of the city of Sahuayo in the northeast corner of the state of Michoacán, in the municipality of Villamar, one kilometer from Alberca Lake (see Figure 3).

ISSN-On line: 2444-4987

In this zone, there are volcanic rocks with andesitic and basaltic compositions, with vitreous augite andesites, lacustrine sediments, and manifestations (Le Bert et al., 2011) such as springs, mud volcanoes, and thermal and fumarole manifestations (Figures 4–6). Photographs were taken with a FLUKE Ti32 IR FUSION TECHNOLOGY industrial thermographic camera to identify and obtain a temperature profile of the geothermal manifestations, using SmartView™ software for their proper handling. The images show a visible light spectrum, an image on the thermal scale, and a 3D image of the isotherms (Figure 7).

Figure 3 Los Negritos, Villamar, Michoacán
Source: Google Earth Adaptation

Figure 4 Spring, Los Negritos
Source: Author's File

Figure 5 Mud Volcano, Los Negritos
Source: Author's File

The operating conditions and considerations beginning at the time of the field visit are seen in Table 1. For the simulation, general equations (eqn. 1–15) for balance were used according to the first law of thermodynamics (Table 2), which were programmed in the Engineering Equation Solver (ESS™). Both evaluated cycles are considered steam cycles, mainly based on the conventional Rankine cycle but with some variations, depending on the cycle that is studied. For the ORC, the cycle is the same; the only difference from the conventional cycle is the working fluid: while the conventional cycle operates with water, the ORC employs a working fluid qualified as organic for its physicochemical characteristics (Figure 8). The Kalina cycle does have some substantial differences; mainly, it uses a binary mixture of ammonia and water in addition to being more complex in its constitution and analysis (Figure 9).

Figure 6 Geothermal Manifestation, Los Negritos
Source: Author's File

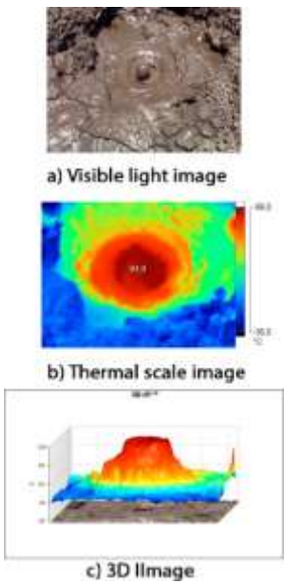

Figure 7 Primary Plain, Los Negritos
Source: Author's File

ISSN-On line: 2444-4987

Temperature of the geothermal source	92 °C
Temperature difference in the steam generator	10 °C
Temperature difference in the condenser	10 °C
Isentropic efficiency of the steam turbine	85 %
Isentropic efficiency of the pump	80 %
Efficiency of the electric generator	96 %
Effectiveness of the steam generator	100 %
Effectiveness of the heat exchanger inside the greenhouse	70 %
Effectiveness of the regenerator (Kalina)	70 %
Mass flow rate of the geothermal fluid	1 kg/s

Table 1 Conditions and Considerations for the ORC and Kalina Cycle Simulations

Equipment	Equation	No.
Pump (OCR)	$W_P = \dot{m}_{WF}(h_2 - h_1)$	1
	$eff_P = \frac{h_{2s} - h_1}{h_2 - h_1}$	2
Pump (Kalina)	$W_P = \dot{m}_{WF}(h_3 - h_2)$	3
	$eff_P = \frac{h_{3s} - h_3}{h_3 - h_3}$	4
Evaporator (OCR)	$\dot{Q}_{in} = \dot{m}_{WF}(h_3 - h_2)$	5
Evaporator (Kalina)	$\dot{Q}_{in} = \dot{m}_5(h_5 - h_4)$	6
Turbine (OCR)	$W_T = \dot{m}_{WF}(h_3 - h_4)$	7
	$eff_T = \frac{h_3 - h_4}{h_3 - h_{4s}}$	8
Turbine (Kalina)	$W_T = \dot{m}_6(h_6 - h_{10})$	9
Condenser (OCR)	$\dot{Q}_{CON} = \dot{m}_{WF}(h_4 - h_1)$	10
Condenser (Kalina)	$\dot{Q}_{CON} = \dot{m}_1(h_1 - h_2)$	11
Electric Generator (ORC y Kalina)	$\dot{W}_{EG} = (\dot{W}_T - \dot{W}_P) * ef_{EG}$	12
Mass Balance	$\sum \dot{m}_{in} - \sum \dot{m}_{out}$	13
Energy Balance	$\sum \dot{E}_{in} - \sum \dot{E}_{out}$	14
Thermal Efficiency	$eff_{th} = \frac{\dot{W}_T - \dot{W}_P}{\dot{Q}_{in}}$	15

Table 2 Equations used for the ORC and Kalina cycle simulations (eqn. 1–15)

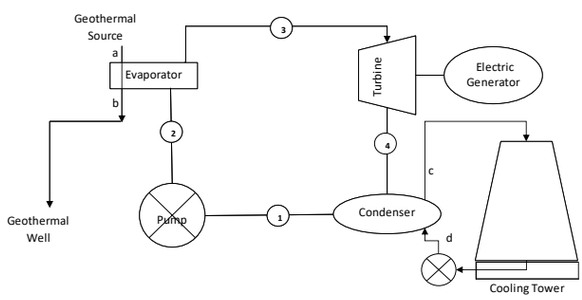

Figure 8 General outline of the organic Rankine cycle

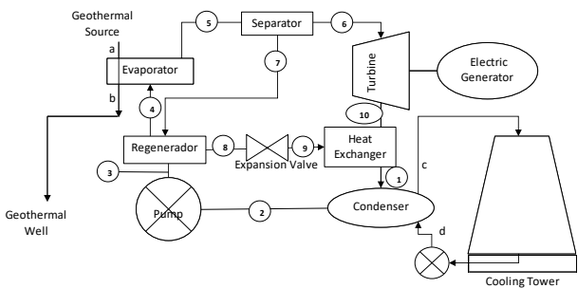

Figure 9 General outline of the Kalina cycle

Results

In the case of the Kalina cycle, before obtaining the results to compare with the ORC, a series of simulations was carried out in which the maximum working pressure and the concentration of ammonia in the mixture varied in order to find the most optimal operating conditions. The results are shown in Table 3. The pressure varied between 10, 20, and 30 bar, while the concentration was between 0.48 and 0.78, with a 0.10 variation for each run. It can be observed that the highest efficiencies were 6.61% at a concentration of 0.48 and a pressure of 10 bar, and an efficiency of 6.80% at a concentration of 0.78 and a pressure of 30 bar. According to these data, the first operating conditions were selected for the work, given that the cost of investment would be lower for having a smaller pump and also needing less replacement working fluid (WF) in the system.

Pressure (bar)	x (Concentration of ammonia in the mixture)	Efficiency of Kalina cycle (%)
10	0.48	6.612
	0.58	4.868
	0.68	2.714
	0.78	1.052
20	0.48	-3.509
	0.58	1.99
	0.68	6.75
	0.78	6.215
30	0.48	-18.7
	0.58	-10.93
	0.68	-5.445
	0.78	6803

Table 3 Comparison of the results of the Kalina cycle simulation in terms of pressure, concentration, and efficiency obtained

The results for each current involved in the ORC are shown in Table 4. Likewise, the results for the Kalina cycle are shown below (Table 5).

ISSN-On line: 2444-4987

No.	P(MPa)	T(°C)	h(kJ/kg)	s(kJ/kg K)
1	0.7487	29.00	92.13	0.3432
2	1.265	29.38	92.68	0.3435
3	1.265	82.00	312.6	1.025
4	0.7487	64.00	301.6	1.025

Table 4 Simulation results of the ORC

No	h (kJ/kg)	P (bar)	Quality (Q_x)	s (kJ/kg K)	T (K)	v (m^3/s)	x (kg/kg)
			P = 10bar x=0.48				
1	152.8	3.175	0.1351	1.127	315.4	0.06462	0.48
2	-109.8	3.175	0	0.2801	302.1	0.00120	0.48
3	-108.8	10	-0.001	0.2808	302.2	0.0012	0.48
4	39.48	10	-0.001	0.7463	335.2	0.00124	0.48
5	321.4	10	0.1381	1.555	355.1	0.02354	0.48
6	1472	10	1	4.893	355.1	0.1628	0.9722
7	137	10	0	1.02	355.1	0.00123	0.4011
8	-35.06	10	-0.001	0.5076	316.6	0.00117	0.4011
9	-35.06	3.175	0.00304	0.5101	315.7	0.0026	0.4011
10	1325	3.175	0.965	4.977	310.7	0.4468	0.9722

Table 5 Simulation results of the Kalina cycle

With the data obtained for both cycles, the next step was to compare the functioning of each set of equipment, where it was observed that the ORC needs more power for the pump (Graphic 1); therefore, it does not only require a higher working power for the cycle, but it also needs a higher mass flow rate of working fluid per unit of geothermal fluid (Graphic 2). For each unit of geothermal fluid, the same amount of working fluid is needed for the ORC, while for the Kalina cycle, only a little less than 0.25 kg of the ammonia-water mixture is needed.

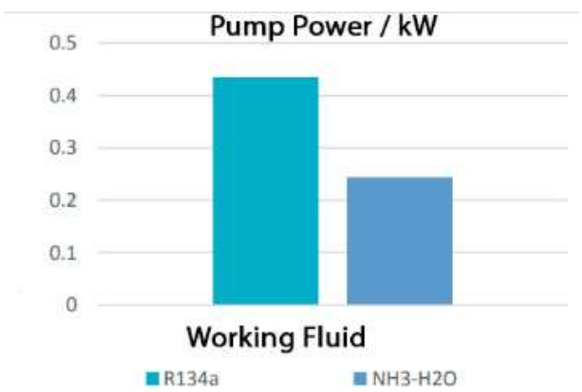

Graphic 1 Power demanded by the pump

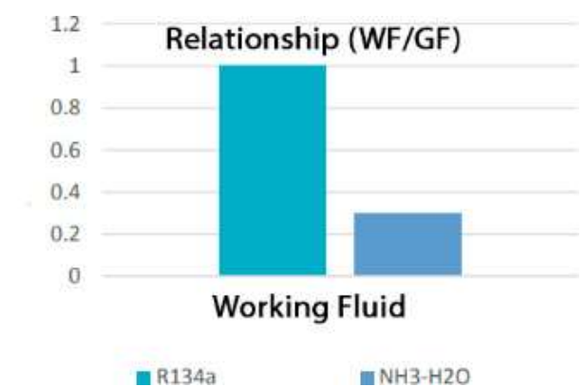

Graphic 2 Mass flow rate of the working fluid in relation to the geothermal fluid

The heat supplied by the geothermal fluid in the part of the steamer can also be considered heat used by the cycle to subsequently be transformed into electrical power. In this area, it can be observed that there is a considerable difference between the heat that one cycle or the other is capable of using; while the heat supplied for the ORC is approximately 220 kWt, the heat used by the Kalina cycle is only 83.58 kWt (Graphic 3). This is most likely because the differences in temperature between the working fluid currents at the steamer's input and output is greater in the ORC compared to in the Kalina. Therefore, the ORC is capable of using the heat better, because when its current 2 reaches the steamer, it has a lower temperature than current 4 of the Kalina cycle; this makes it susceptible to absorbing a higher amount of heat for the cycle.

In the case of the net power output of both cycles and the efficiency obtained respectively, it can be observed that while the Kalina cycle's efficiency (6.61%) was higher than the ORC's efficiency (4.58%), the power output does not behave in the same way (10.54 kWe and 5.77 kWe, respectively), as observed in Graphic 4 and 5.

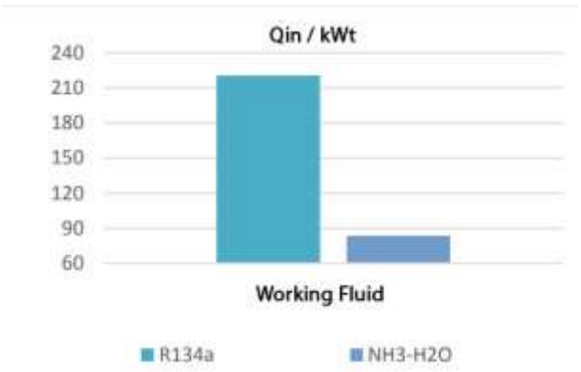

Graphic 3 Heat supplied in the steamer

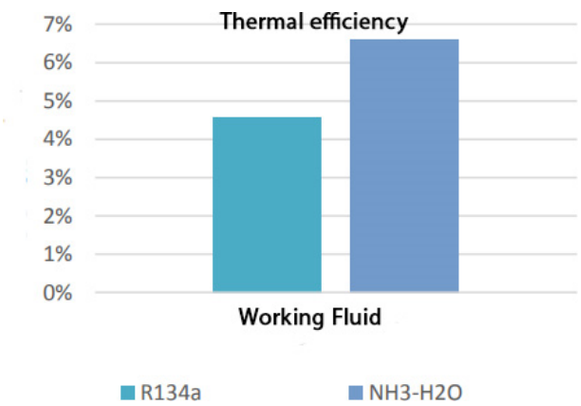

Graphic 4 Thermic efficiency obtained for the ORC and Kalina cycle

ISSN-On line: 2444-4987

Even though the Kalina cycle was more efficient, it does not produce more power than the ORC. This is because the heat in the steamer that can be used by the ORC is much higher than that used by the Kalina cycle. This is due to the cycles' internal operating conditions and the conditions that this low-enthalpy geothermal source presents, since the geothermal fluid can only transfer heat to the working fluid at a temperature of 82° C.

A more exhaustive analysis could demonstrate more clarity on the latter fact, especially if analyzed according to the second law of thermodynamics, since this would make it possible to observe which of the two cycles destroys more exergy.

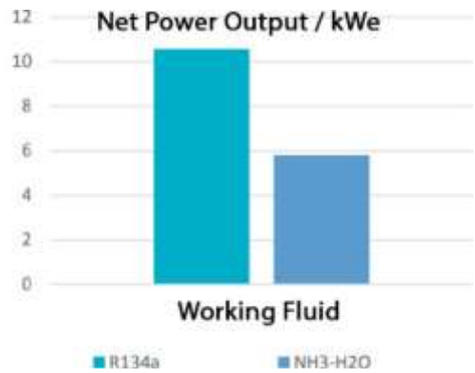

Graphic 5 Net power output for both cycles

Conclusions

The analysis indicates that these types of electric power generation plants are possible alternatives for low enthalpy sources, as in the case of the town of Los Negritos, Michoacán. Also, it was detected that while the Kalina cycle has higher thermic efficiency than the ORC cycle, the net power output was greater for the latter. This is attributed to the temperature difference in the steamer; on the cycle side, it is higher for the ORC than for the Kalina. That said, the heat used by the ORC in the steamer is considerably greater than what is used in the Kalina cycle. More exhaustive studies of the analyzed conditions are needed in order to determine the benefits of these cycles.

Referencies

Abrigo, S. A. (2022). *Identificación y aprovechamiento de los recursos energéticos renovables en la provincia del Neuquén, su impacto en la matriz energética de generación eléctrica y socio-económico de escala regional.* (Master). Universidad Nacional del Comahue, Retrieved from http://rdi.uncoma.edu.ar/handle/uncomaid/16716

Fridleifsson, I. B. (2001). Geothermal energy for the benefit of the people. *Renewable and sustainable energy reviews, 5*(3), 299-312. doi:https://doi.org/10.1016/S1364-0321(01)00002-8

Gómez-Tuena, A., Orozco-Esquivel, M., & Ferrari, L. (2005). Petrogénesis ígnea de la faja volcánica transmexicana. *Boletín de la Sociedad geológica Mexicana, 57*(3), 227-283. doi:https://doi.org/10.18268/bsgm2005v57n3a2

Huttrer, G. W. (2020). *Geothermal power generation in the world 2015-2020 update report*. Paper presented at the Proceedings world geothermal congress, Reykjavik, Iceland. https://www.geothermal-energy.org/pdf/IGAstandard/WGC/2020/01017.pdf

Le Bert, G. H., Gutiérrez-Negrín, L., Quijano León, H., Ornelas Celis, A., Espíndola, S., & Hernandez Carrillo, I. (2011). *Evaluación de la energía geotérmica en México*. Retrieved from https://www.cre.gob.mx/documento/2026.pdf

Madhawa Hettiarachchi, H., Golubovic, M., Worek, W. M., & Ikegami, Y. (2007). The performance of the Kalina cycle system 11 (KCS-11) with low-temperature heat sources. *J. Energy Resour. Technol., 129*(243–247). doi:https://doi.org/10.1115/1.2748815

Martínez R. J., V. R. I., Estrada J. M., Ortiz S. A., Moreno N. I., Montes A.F.G., F. García Á., Mendez R. E. (2014). Geochemical Prospection of the Chapala Ciénega at Michoacán State. *International Journal of Geosciences, 5*(9), 5. doi:http://dx.doi.org/10.4236/ijg.2014.59086

ISSN-On line: 2444-4987

Molés, F., Navarro-Esbrí, J., Peris, B., Mota-Babiloni, A., & Kontomaris, K. K. (2015). Thermodynamic analysis of a combined organic Rankine cycle and vapor compression cycle system activated with low temperature heat sources using low GWP fluids. *Applied Thermal Engineering, 87*, 444-453. doi:https://doi.org/10.1016/j.applthermaleng.2015.04.083

Noorollahi, Y., Shabbir, M. S., Siddiqi, A. F., Ilyashenko, L. K., & Ahmadi, E. (2019). Review of two decade geothermal energy development in Iran, benefits, challenges, and future policy. *Geothermics, 77*, 257-266. doi:https://doi.org/10.1016/j.geothermics.2018.10.004

Palomo-Torrejón, E., Colmenar-Santos, A., Rosales-Asensio, E., & Mur-Pérez, F. (2021). Economic and environmental benefits of geothermal energy in industrial processes. *Renewable Energy, 174*, 134-146. doi:https://doi.org/10.1016/j.renene.2021.04.074

SENER. (2021). *BALANCE NACIONAL DE ENERGÍA 2020*. MÉXICO: SECRETARIA DE ENERGÍA Retrieved from https://www.gob.mx/cms/uploads/attachment/file/707654/BALANCE_NACIONAL_ENERGIA_0403.pdf

SIE. (2022). SISTEMA DE INFORMACIÓN ENERGÉTICA Geoenergía. Retrieved from https://sie.energia.gob.mx/bdiController.do?action=temas.

Vera-Romero, I., Corona-Ruíz, S. L., Reyes, J. M., Nava, I. M., & Murillo, O. O. (2018). Comparación térmica de un Ciclo Rankine Orgánico accionado por una fuente geotérmica de calor de baja temperatura. *CONGRESO INTERNACIONAL ANUAL DE LA SOMIM*. Retrieved from http://somim.org.mx/memorias/memorias2018/articulos/A4_120.pdf

Villeda, M. S., Zúñiga, I. Y. C., & Flores, M. D. R. S. (2021). El Desarrollo Energético Sostenible en el Mundo y en México. El caso de la energía geotérmica. *Repositorio de la Red Internacional de Investigadores en Competitividad, 15*(15), 1372-1387. Retrieved from https://www.riico.net/index.php/riico/article/view/2047/1853

ISSN-On line: 2444-4987

Article **Journal of Research and Development**
June 2022, Vol.8 No.21 21-27

Design and automation of an electrospinning system to prepare micro and nanofibers. Case study: elaboration of polymeric micro and nanofibers for vaginal drug delivery

Diseño y automatización de un sistema de electrohilado para la preparación de micro y nanofibras. Estudio de caso: Elaboración de micro y nanofibras poliméricas de administración vaginal

MARTÍNEZ-PÉREZ, Beatriz´†*, OLIVANO-ESQUIVEL, Ana Daniela´, FERNÁNDEZ-RETANA, Jorge´ and VIDAL-ROMERO, Gustavo´´

´*Universidad Politécnica del Valle de México. División de Ingeniería en Nanotecnología. México*
´´*Universidad Nacional Autónoma de México, Laboratorio de Posgrado en Tecnología Farmacéutica, Facultad de Estudios Superiores Cuautitlán, Estado de México C.P. 54745, México*

ID 1st Author: *Beatriz, Martínez-Pérez* / **ORC ID:** 0000-0003-0277-0028, **CVU CONACYT ID:** 214825

ID 1st Co-author: *Ana Daniela, Olivano-Esquivel* / **ORC ID:** 0000-0002-7306-5812

ID 2nd Co-author: *Jorge, Fernández-Retana* / **ORC ID:** 0000-0002-8282-3865, **CVU CONACYT ID:** 104639

ID 3rd Co-author: *Gustavo, Vidal-Romero* / **ORC ID:** 0000-0002-2706-3429, **CVU CONACYT ID:** 472862

DOI: 10.35429/JRD.2022.21.8.21.27 Received: January 30, 2022; Accepted: May 30, 2022

Abstract

In the present investigation was optimized and automated a prototype of an electrospinning system. In addition, the methodology for preparing the polymeric film with polycaprolactone micro and nanofibers (PCL) loaded with Neem extract was optimized as a proposal for the treatment of cervical cancer. Also, a UV-VIS spectrophotometric method was developed for the quantification of Neem extract encapsulated in PCL polymeric nanofibers through the formation of a colorimetric complex with FeCl3. The wavelength used to quantify the Neem extract was 423 nm. The prototype built allowed the formation of nanofibers loaded with Neem extract with a diameter of 22-71 nm in diameter. The encapsulation efficiency of the Neem extract was 78.4%.

Electrospinning, Cervicouterine cancer, Polymeric membrane

Resumen

En el presente trabajo se optimizó y automatizó un prototipo de sistema de electrohilado. El sistema de electrohilado, nos permitió preparar una membrana polimérica no tejida con micro y nanofibras de policaprolactona (PCL) cargadas con extracto Neem como alternativa para el tratamiento de cáncer cervicouterino. Además, se desarrolló un método espectrofotométrico UV-VIS para la cuantificación de extracto de Neem encapsulado en las nanofibras poliméricas de PCL por medio de la formación de un complejo colorimétrico con FeCl3. La longitud de onda utilizada para cuantificar el extracto de Neem fue de 423 nm. El prototipo construido permitió la formación de nanofibras cargadas con extracto de Neem con un diámetro de 22-71 nm. La eficiencia de encapsulación del extracto de Neem fue de 78.4%.

Electrohilado, Cáncer cervicouterino, Membrana polimérica

Citation: MARTÍNEZ-PÉREZ, Beatriz, OLIVANO-ESQUIVEL, Ana Daniela, FERNÁNDEZ-RETANA, Jorge and VIDAL-ROMERO, Gustavo. Design and automation of an electrospinning system to prepare micro and nanofibers. Case study: elaboration of polymeric micro and nanofibers for vaginal drug delivery. Journal of Research and Development. 2022. 8-21:21-27.

* Author's Correspondence (E-mail: beatriz.martinez@upvm.edu.mx)
† Researcher contributing as first author.

Introduction

Cervical cancer is a health problem with a high mortality rate. Specifically, Mexico occupies the second place in cases, behind breast cancer. Its high incidence is related to ignorance and low culture of prevention, since this cancer is detectable, and if discovered in a timely manner, the chances of curing it are high.

According to the World Health Organization (WHO), there are more than 6 million cases of cancer in women; 57.2% of these cases occur in developing countries. In Mexico, cervical cancer is the second leading cause of cancer death in women. Annually, there is an estimated occurrence of 13,960 cases in women, with an incidence of 23.3 cases per 100,000 women (CNEGSR, 2016). Cervical cancer is multicausal and is due to the association of different risk factors. One of the main causes is human papillomavirus (HPV) infection. Co-infections of HPV with other sexually transmitted infectious agents, such as *Chlamydia trachomatis*, herpes simplex virus type 2 (HSV-2) and human immunodeficiency virus (HIV) possibly condition a synergistic effect that increases the chances of cellular alterations leading to the development of a neoplasm. *Chlamydia trachomatis* infection and marginally HVS-2 favor the entry and persistence of multiple HPV types, leading to viral integration, inhibition of apoptosis, overexpression of E6/E7 oncogenes and cellular transformation (Hernández-Hernández *et al*., 2015).

In addition, some of the causes of the presence of cancer are aggravated or originate from other vaginal infections. As of 2014 in Mexico, during reproductive age 75% of women experience at least one episode of vulvovaginal candidiasis. Approximately 6 to 55% of healthy women are asymptomatic carriers (Solís-Árias *et al*., 2014). Vulvovaginal candidiasis is a very common infection affecting at least 50% of women once in their lifetime; it accounts for 25% of total vaginal infections. Recurrences are frequent and it has been estimated that 50% of cases will present a second episode after the first clinical picture (Martinez-Perez *et al*., 2018). There are several cytotoxic drugs used in the treatment of cervical cancer, which present many adverse effects that are derived from the use of high doses and/or due to the lack of specificity in the therapeutic target.

Nanotechnology offers a series of opportunities for pharmaceutical innovation, by exploring new routes of administration that are less aggressive and more comfortable for the patient through the development of different therapeutic nanosystems, nanofibers, nanoparticles, nanocapsules, etc. Offering the possibility of significantly improving treatment schemes with a modified release of active molecules. The advantages of nanosystems such as: protection of labile drugs, controlled release, modulation of adhesion and/or penetration to vaginal mucus; offer a great opportunity for their application in vaginal drug delivery (Nunes *et al*., 2021). Nanofibers are an example of these nanosystems, generally possessing a diameter of less than 1000 nm, reaching even kilometer lengths (Zhang *et al*., 2018). Currently, their interest and research is increasing because they have the following advantages: greater surface area that allows greater interpenetration; high bioadhesive strength, which allows longer contact time and controlled release of active ingredients; easier and more comfortable administration for patients (Machado *et al*., 2016).

There are different techniques for obtaining nanofibers, which are limited by the type of material, type of solvents, manufacturing times and low process efficiency. For example, by controlling process factors such as applied voltage or flow rate of the solutions, it is possible to control nanofiber characteristics such as porosity, specific surface area, mechanical strength and morphology (Sanabria-Romero F., 2022). The electrospinning process is simple and has the following stages: a polymeric solution is contained in an injection syringe, the metal tip of the injection system is connected to a high voltage source (5-50kV), when the electric field is able to overcome the surface tension of the polymeric solution droplet deforming it to a conical "Taylor cone" tip, the polymeric solution starts to flow as a distorted jet which is attracted and electrically deposited on a collector plate as solid fibers, forming a polymeric membrane on the collector (Figure 1) (Velasco-Baraza *et al*., 2016).

ISSN-On line: 2444-4987

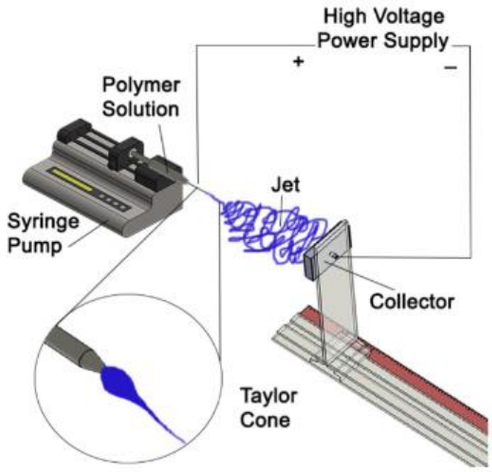

Figure 1 Electrospinning configuration system
Source: (Velasco-Baraza et al., 2016)

In this research work, it is proposed to obtain polymeric nanofibers as a delivery system for Neem (*Azadirachta indica*) extract due to its cytotoxic properties to combat cervical cancer. According to studies by Avalos-Soto *et al*. (2014), ethanolic extracts of *A. indica* showed toxic and cytotoxic activity, being the ethanolic extract of Neem seed the one that presented the highest toxic activity with an LD50 of 476 µg/ml on *A. indica* nauplii, regarding cytotoxic activity the crude extract of Neem leaf was the one that presented the highest activity with an IC50 of 22. 03 µg/ml on the MCF7 line (breast cancer), the hexane fraction of Neem leaf was the most active on the MCF7 cell line (breast cancer) with an IC50 of 25.17 µg/ml; these results allow us to consider it as a potential adjuvant in the treatment of cancer. Therefore, the objective of the present work is to design and automate a horizontal electrospinning system to elaborate a polymeric membrane with nano and microfibers of prolonged release of Neem extract as an alternative for the treatment of cervical cancer.

Materials and Methods

Materials

Poly-ε-caprolactone (PCL) (P.M. 80,000) was purchased from Química, S. de RL. de CV (Mexico). Neem extract was purchased from Extractos Sigma S. A. de C. V. (Mexico). ACS glacial acetic acid and reagent grade acetone were purchased from Fermont® (Mexico). 5 ml sterile syringes with 21G gauge needles and 32 mm length were used. Electronic components from disused computers and printers were recycled for the construction of the electrospinner.

Equipment

UV-Vis spectrophotometer (Thermo Scientific, Genesys 10uv Scanning, USA), inverted platinum optical microscope, (Carl Zeizz, M. AX10Vert.A1, Mexico).

Experimental Methods

Construction of the electrospinning system

Recycled parts were collected from electronic devices: *flayback* (computer monitor), electricity saving light bulb circuit, printer roller, motor and syringes. The parts were assembled on an acrylic platform according to the electrospinning system scheme (Figure 1). Previously the recycled parts such as *flayback*, printer roller and motor were cleaned with alcohol.

Automation of the electrospinning system

The movement of the infusion pump from right to left was automated to avoid agglomeration of the fibers at the time of injection, installing an Arduino board controlled by means of an algorithm to establish the direction and speed of rotation of motors with an L293D driver. The movement of the collector plate was controlled by a 5V motor connected directly to the power outlet with a 5V eliminator. A U.V. lamp was also installed on top of the system for aseptic conditions. The voltage source (*flayback*) was obtained from an old computer monitor, with 10 and 15 Kv characteristics.

Fabrication of polymeric micro and nanofibers

A polymeric solution was prepared employing poly-ε-caprolactone (16.66 % (w/v)) and 50 mg of Neem extract, using acetone as solvent. A blank polymeric solution was prepared at the same concentration, without the addition of extract. The prepared polymeric solution was deposited in a 5 ml syringe coupled with a 21G X 32 mm gauge metal needle. The polymeric solution was injected under continuous flow, using a voltage of 10 kV at a distance of 10 cm from the collector plate, which was covered with aluminum foil where the nanofibers were deposited**.**

ISSN-On line: 2444-4987

Morphology

Fiber morphology and size were determined by means of an inverted optical microscope (Zeiss), employing a 1000 X magnifying eyepiece. The morphology of poly-ε-caprolactone fibers (PCL-NFs) and poly-ε-caprolactone fibers with Neem extract (PCL-NEEM-NFs) was evaluated.

Encapsulation efficiency of Neem extract

Samples of 50-100 mg of the polymeric membrane were hydrolyzed with 3 ml of [1.3 M] HCl for 48 hours. Subsequently, the samples were neutralized with NaOH [2.5 M]. The systems were filtered with a Millipore 0.22 µm membrane. The filtrate obtained was made up to 10 ml using an 8% (w/v) sodium lauryl sulfate solution (LSS) as solvent (Solution A). Aliquots of 5 ml of Solution A were taken and 20 µl of a 0.5% (w/v) $FeCl_3$ acid solution (Solution B) were added. This solution was heated to a temperature of 60°C for 15 min, allowed to cool to room temperature and its absorbance was determined at a maximum wavelength (λ) of 423 nm.

The amount of loaded extract was obtained from the formula 1:

$$\%E.C.=(CE/CEI)*100 \quad (1)$$

Where E.C., is the amount of extract loaded on the polymeric membrane, C.E, is the amount of loaded extract determined and C.E.I., is the amount of initial extract.

Results and discussion

Construction and automation of the electrospinning system

Figure 3 shows the final prototype of the automated electrospinning system. As a result, a fixed structure was obtained for the injection pump by means of rails, through which the direction and form of injection of the polymeric solutions on the collector plate can be controlled. An Arduino system controlled by a cell phone was coupled to control the injection speed of the infusion pump.

Figure 2 PCL polymeric membranes obtained by the electrospinning technique

Fabrication of polymeric micro and nanofibers

The assembly of the electronic components to assemble the electrospinning prototype was adequate, using such equipment polymeric membranes of poly-ε-caprolactone were obtained. The dimensions of the films formed were 17 x 17 cm in area (Figure 2).

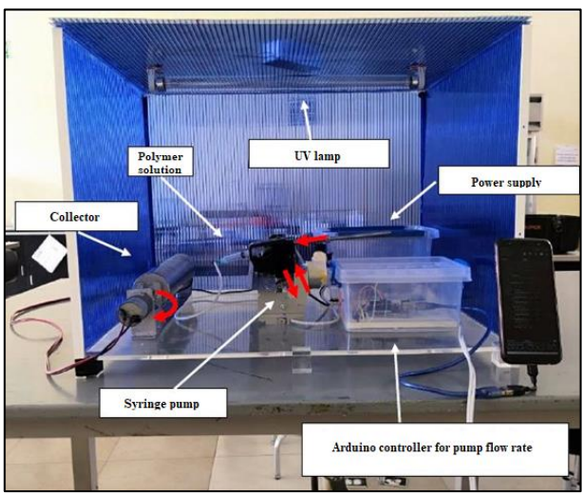

Figure 3 Automated electrospinnng system for obtaining polymeric membranes

Morphology

As shown in Figure 4, the PCL-NFs obtained have a diameter of 28-35 nm. The micrograph of the polymer film indicates a variation between the sizes of the nanofibers, this may be due to the lack of control of the injection rate of the polymer solution, a factor that will be considered for the formation of the following membranes.

ISSN-On line: 2444-4987

In Figure 5, the polymeric membrane containing Neem extract presents a greater thickness and therefore a larger diameter of the fibers (22-71 nm). This may be due to the presence of the extract, due to an increase in the viscosity of the solution to be injected. However, despite having control over the injection rate, the polymeric membrane still continues to form with differences in nanofiber sizes. This suggests the need to control the injection distance, as well as to control parameters of the polymeric solution, such as: viscosity, type of solvent, concentration, conductivity, among others.

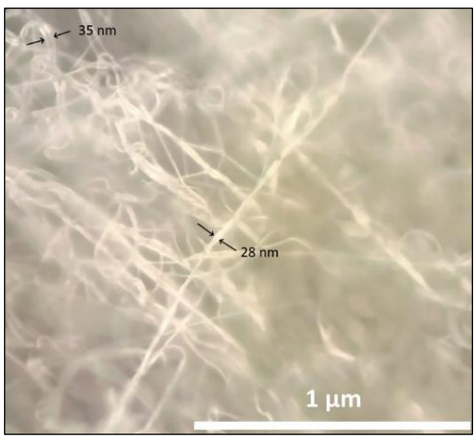

Figure 4 Optical micrograph of the polymeric membrane PCL-NFs. Images taken with a Carl Zeiss inverted optical microscope at 1000x magnification

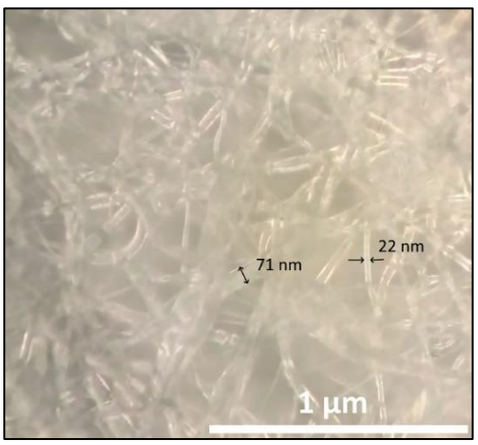

Figure 5 Optical micrograph of the polymeric membrane PCL-NEEM-NFs. Images taken with a Carl Zeiss inverted optical microscope, at 1000x magnification

According to the results, the prototype electrospinning equipment presents some limitations that can be modified and adapted, such as: a) the power supply has a maximum voltage of 15 KV, b) the size of the fibers is dependent on the power of the power supply.

Neem extract encapsulation efficiency

In Graphic 1, the UV-VIS absorption spectrum of the 0.5% Neem extract-FeCl3 colored complex is shown. The absorption maximum occurred at a wavelength of 423 nm. According to Fong Lores et al. (2014), Neem extract, can form colored complex with $FeCl_3$ to determine phenols and tannins, in this study, the colored complex of Neem extract with $FeCl_3$ was formed to quantify its content present in PCL-NEEM-NFs.

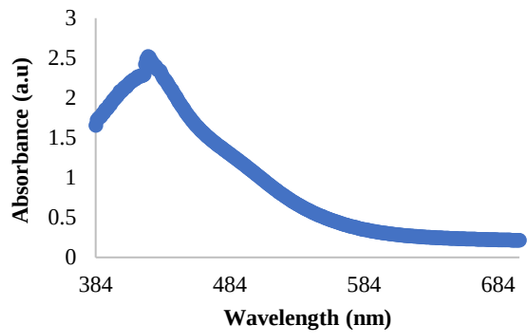

Graphic 1 UV-Vis spectrum of the colored complex of Neem-$FeCl_3$ at 0.5%

Graphic 2 shows the linear relationship between the concentration of the colored complex of Neem-$FeCl_3$ extract at 0.5% and its absorbance, in the concentration range of 0.10 to 0.51 mg/ml (r^2=0.99). In Table 1, the results of the calibration curve have a coefficient of variation of 2.24% less than 3%, a criterion established in the Guide for the Validation of Analytical Methods (Garcia et al., 2002), these values indicate that the method is reliable for quantifying the concentration of Neem extract on the polymeric membrane.

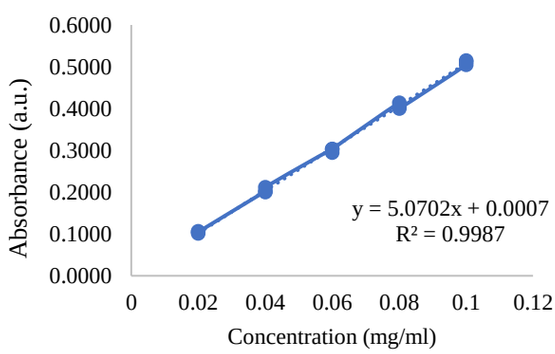

Graphic 2 Calibration curve of the 0.5% Neem-$FeCl_3$ colored complex (λ=423nm)

ISSN-On line: 2444-4987

Concentration (mg/ml)	Absorbance	Abs/conc
0.02	0.1009	5.05
0.02	0.1063	5.32
0.02	0.1048	5.24
0.04	0.2019	5.05
0.04	0.1998	4.99
0.04	0.2115	5.29
0.06	0.3028	5.05
0.06	0.2945	4.91
0.06	0.3026	5.04
0.08	0.4137	5.17
0.08	0.4041	5.05
0.08	0.3997	4.99
0.1	0.5046	5.05
0.1	0.5148	5.15
0.1	0.5115	5.12
	Average	**5.09**
	Stand. Deviation	**0.11**
	%C.V.	**2.25**
Note: C.V. Coefficient of variation		

Table 1 Calibration curve to evaluate the linearity of the UV-VIS spectrophotometric method for the quantification of Neem-$FeCl_3$ at 0.5% (λ=423nm)

The calibration curve allowed us to quantify the amount of Neem extract loaded on the polymeric membrane. The percentage of encapsulation efficiency was 78.4%, a favorable result, however, further studies will be necessary considering a higher load of extract to be loaded on the polymeric nanofibers.

Conclusions

A prototype of electrospinning equipment was built and automated from recycled parts of electronic components. The prototype allowed us to obtain a polymeric membrane of PCL-NEEM- NFs, with diameters in the range of 22-71 nm. The variation in the average diameter of the nanofibers suggests that it is necessary to have greater control over the infusion rate of the polymeric solution to obtain more homogeneous fiber diameters, in addition to the need to correlate the parameters of the polymeric solution to optimize the obtaining of homogeneous membranes. The method to quantify the Neem extract in PCL-NEEM-NFs allowed us to determine that we were able to obtain 78.4% encapsulation efficiency. The PCL-NEEM-NFs film may be a viable alternative for cytotoxicity studies with cervical cancer cell models.

Acknowledgments

This work was funded by the Consejo de Ciencia y Tecnología del Estado de México (COMECyT) under project FICDTEM-2021-050.

References

Ávalos-Soto J., Treviño-Neávez J.F., Verde-Star M.J., Rivas-Morales C., Oranday-Cárdenas A., Moran-Martínez J., Serrano-Gallardo L.B., Morales Rubio M.E. 2014. Evaluación citotóxica de los extractos etanólicos de *Azadirachta indica* (A. Juss) sobre diferentes líneas celulares. *Rev. Mex. Cienc. Farm*. 45(3). Recuperado en 19 de septiembre de 2022, de https://www.scielo.org.mx/scielo.php?script=sci_arttext&pid=S1870-01952014000300004&lng=es&tlng=es

Comisión Nacional de Equidad de Género y Salud Reproductiva (CNEGSR). 2016. Hoja de datos sobre cáncer de cuello uterino. Secretaría de Prevención y Promoción de la Salud. Recuperado en 05 de septiembre de 2022, de: http://cnegsr.salud.gob.mx/contenidos/descargas/CaCu/HojadatosCancerdeCuelloUterino2016.pdf

Fong Lores O., Berenguer Rivas C., Jorge de la Vega A., Wawoe Díaz N., Puente Zapata E. 2014. Potencial antioxidante de un extracto acuoso de hojas de NIM (*Azadirachta Indica A. Juss*). *Rev. Cub. Plan. Med*. 19(2). Recuperado en 19 de septiembre de 2022, de https://www.medigraphic.com/cgi-bin/new/resumen.cgi?IDARTICULO=53773

García M. A., Soberón E., Cortés M., Rodríguez R., Herrera L., Alcantará A. 2002. Métodos Analíticos. Guía de Validación. Colegio Nacional de Químicos Farmacéuticos Biólogos México, *A. C. (CNQFBM).*

Hernández-Hernández D. M., Apresa-García T., Patlán-Pérez R. M. 2015. Panorama epidemiológico del cáncer cervicouterino. *Rev. Med. Inst. Mex. Seguro Soc.* 53(2), 154-161. https://www.redalyc.org/articulo.oa?id=457744942006

ISSN-On line: 2444-4987

Machado A., Cunha-Reis C., Araújo F., Nunes R., Seabra V., Ferreira D., das Neves J., Sarmento B. 2016. Development and *in vivo* safety assessment of tenofovir-loaded nanoparticles-in-film as a novel vaginal microbicide delivery system. *Acta Biomaterialia. 44,* 332-340. DOI: https://doi.org/10.1016/j.actbio.2016.08.018

Martínez-Pérez B., Quintanar-Guerrero D., Tapia-Tapia M., Cisneros-Tamayo R., Zambrano-Zaragoza M. L., Alcalá-Alcalá S., Mendoza-Muñóz N., Piñón-Segundo E. 2018. Controlled-release biodegradable nanoparticles: From preparation to vaginal applications. *Eur. J. Pharm. Sci.* 115, 1485-195. DOI: https://doi.org/10.1016/j.ejps.2017.11.029

Nunes R., Bogas S., Faria M. J., Gonçalves H., Lúcio M., Viseu T., Sarmento B., das Neves J. (2021). Electrospun fibers for vaginal administration of tenofovir disoproxil fumarate and emtricitabine in the context of topical pre-exposure prophylaxis. *J. Control. Release,* 334, 453-462. DOI: https://doi.org/10.1016/j.jconrel.2021.05.003

Sanabria-Romero F. 2022. Desarrollo de membranas de quitosano-aloe vera y quitosano-triticum vulgare con posibles aplicaciones biomédicas. Tesis. Universidad Autónoma de Querétaro. Recuperado en 19 de septiembre de 2022, de http://ri-ng.uaq.mx/handle/123456789/3779

Solís-Árias M. P., Moreno-Morales M., Dávalos-Tanaka M., Fernández-Martínez R. F., Díaz-Flores O., Arenas-Gúzman R. 2014. Colonización vaginal por *Candida spp*. Frecuencia y descripción de las especies aisladas en mujeres asintomáticas. *Ginecol. Obstet. Mex*. 82, 1-8. Recuperado en 19 de septiembre de 2022, de https://ginecologiayobstetricia.org.mx/articulo/colonizacion-vaginal-por-candida-spp-frecuencia-y-descripcion-de-las-especies-aisladas-en-mujeres-asintomaticas

Velasco-Baraza R.D., Álvarez Suarez A.S., Villarreal Gómez L.J., Paz González J.A., Iglesias A.L., Vera Graziano R. 2016. Designing a Low Cost Electrospinning Device for Practical Learning in a Bioengineering Biomaterials Course. *Rev. Mex. Ing. Biomed*. 37(1). DOI: https://doi.org/10.17488/RMIB.37.1.1

Zhang L., Jia Y., He H., Juliang Y., Ruoyang C., Caiqian C., Shen W., Wang X. 2018. Multiple Factor Analysis on Preparation of Cellulose Nanofiber by Ball Milling from Softwood Pulp. *Bioresources*. 13, 2397-2410. Recuperado en 19 de septiembre de 2022, de https://ojs.cnr.ncsu.edu/index.php/BioRes/article/view/13033.

ISSN-On line: 2444-4987

[Title in Times New Roman and Bold No. 14 in English and Spanish]

Surname (IN UPPERCASE), Name 1st Author†*, Surname (IN UPPERCASE), Name 1st Coauthor, Surname (IN UPPERCASE), Name 2nd Coauthor and Surname (IN UPPERCASE), Name 3rd Coauthor

Institutional Affiliation of Author including Dependency (No.10 Times New Roman and Italic)

International Identification of Science - Technology and Innovation

ID 1st Author: (ORC ID - Researcher ID Thomson, arXiv Author ID - PubMed Author ID - Open ID) and CVU 1st author: (Scholar-PNPC or SNI-CONACYT) (No.10 Times New Roman)

ID 1st Coauthor: (ORC ID - Researcher ID Thomson, arXiv Author ID - PubMed Author ID - Open ID) and CVU 1st coauthor: (Scholar or SNI) (No.10 Times New Roman)

ID 2nd Coauthor: (ORC ID - Researcher ID Thomson, arXiv Author ID - PubMed Author ID - Open ID) and CVU 2nd coauthor: (Scholar or SNI) (No.10 Times New Roman)

ID 3rd Coauthor: (ORC ID - Researcher ID Thomson, arXiv Author ID - PubMed Author ID - Open ID) and CVU 3rd coauthor: (Scholar or SNI) (No.10 Times New Roman)

(Report Submission Date: Month, Day, and Year); Accepted (Insert date of Acceptance: Use Only ECORFAN)

Abstract (In English, 150-200 words)

Objectives
Methodology
Contribution

Keywords (In English)

Indicate 3 keywords in Times New Roman and Bold No. 10

Abstract (In Spanish, 150-200 words)

Objectives
Methodology
Contribution

Keywords (In Spanish)

Indicate 3 keywords in Times New Roman and Bold No. 10

Citation: Surname (IN UPPERCASE), Name 1st Author, Surname (IN UPPERCASE), Name 1st Coauthor, Surname (IN UPPERCASE), Name 2nd Coauthor and Surname (IN UPPERCASE), Name 3rd Coauthor. Paper Title. Journal of Research and Development. Year 1-1: 1-11 [Times New Roman No.10]

* Correspondence to Author (example@example.org)
† Researcher contributing as first author.

Introduction

Text in Times New Roman No.12, single space.

General explanation of the subject and explain why it is important.

What is your added value with respect to other techniques?

Clearly focus each of its features

Clearly explain the problem to be solved and the central hypothesis.

Explanation of sections Article.

Development of headings and subheadings of the article with subsequent numbers

[Title No.12 in Times New Roman, single spaced and bold]

Products in development No.12 Times New Roman, single spaced.

Editable

In the article content any graphic, table and figure should be editable formats that can change size, type and number of letter, for the purposes of edition, these must be high quality, not pixelated and should be noticeable even reducing image scale.

[Indicating the title at the bottom with No.10 and Times New Roman Bold]

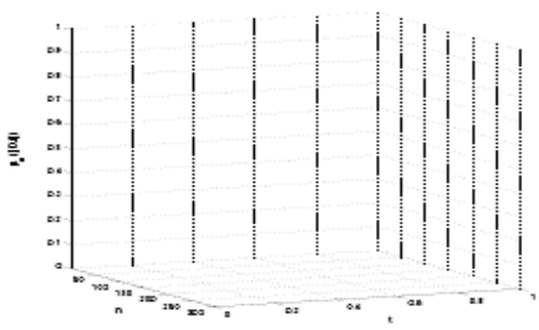

Graphic 1 Title and *Source (in italics)*

Should not be images-everything must be editable.

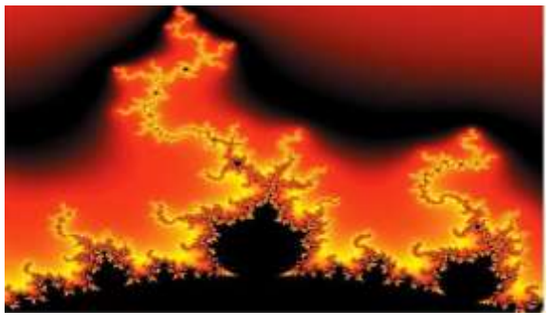

Figure 1 Title and *Source (in italics)*

Should not be images-everything must be editable.

Table 1 Title and *Source (in italics)*

Should not be images-everything must be editable.

For the use of equations, noted as follows:

$$Y_{ij} = \alpha + \sum^{r} \quad \beta_h X_{hij}$$

Must be editable and number aligned on the right side.

Methodology

Develop give the meaning of the variables in linear writing and important is the comparison of the used criteria.

Results

The results shall be by section of the article.

Annexes

Tables and adequate sources

Thanks

Indicate if they were financed by any institution, University or company.

Conclusions

Explain clearly the results and possibilities of improvement.

ISSN 2444-4987

References

Use APA system. Should not be numbered, nor with bullets, however if necessary numbering will be because reference or mention is made somewhere in the Article.

Use Roman Alphabet, all references you have used must be in the Roman Alphabet, even if you have quoted an Article, book in any of the official languages of the United Nations (English, French, German, Chinese, Russian, Portuguese, Italian, Spanish, Arabic), you must write the reference in Roman script and not in any of the official languages.

Technical Specifications

Each article must submit your dates into a Word document (.docx):

Journal Name
Article title
Abstract
Keywords
Article sections, for example:

1. Introduction
2. Description of the method
3. Analysis from the regression demand curve
4. Results
5. Thanks
6. Conclusions
7. References

Author Name (s)
Email Correspondence to Author
References

Intellectual Property Requirements for editing:

- Authentic Signature in Color of Originality Format Author and Coauthors.

- Authentic Signature in Color of the Acceptance Format of Author and Coauthors.

- Authentic Signature in blue Color of the Conflict of Interest Format of Author and Co-authors.

Reservation to Editorial Policy

Journal of Research and Development reserves the right to make editorial changes required to adapt the Articles to the Editorial Policy of the Journal. Once the Article is accepted in its final version, the Journal will send the author the proofs for review. ECORFAN® will only accept the correction of errata and errors or omissions arising from the editing process of the Journal, reserving in full the copyrights and content dissemination. No deletions, substitutions or additions that alter the formation of the Article will be accepted.

Code of Ethics - Good Practices and Declaration of Solution to Editorial Conflicts

Declaration of Originality and unpublished character of the Article, of Authors, on the obtaining of data and interpretation of results, Acknowledgments, Conflict of interests, Assignment of rights and Distribution

The ECORFAN-Mexico, S.C Management claims to Authors of Articles that its content must be original, unpublished and of Scientific, Technological and Innovation content to be submitted for evaluation.

The Authors signing the Article must be the same that have contributed to its conception, realization and development, as well as obtaining the data, interpreting the results, drafting and reviewing it. The Corresponding Author of the proposed Article will request the form that follows.

Article title:

– The sending of an Article to Journal of Research and Development emanates the commitment of the author not to submit it simultaneously to the consideration of other series publications for it must complement the Format of Originality for its Article, unless it is rejected by the Arbitration Committee, it may be withdrawn.

– None of the data presented in this article has been plagiarized or invented. The original data are clearly distinguished from those already published. And it is known of the test in PLAGSCAN if a level of plagiarism is detected Positive will not proceed to arbitrate.

– References are cited on which the information contained in the Article is based, as well as theories and data from other previously published Articles.

– The authors sign the Format of Authorization for their Article to be disseminated by means that ECORFAN-Mexico, S.C. In its Holding Spain considers pertinent for disclosure and diffusion of its Article its Rights of Work.

– Consent has been obtained from those who have contributed unpublished data obtained through verbal or written communication, and such communication and Authorship are adequately identified.

– The Author and Co-Authors who sign this work have participated in its planning, design and execution, as well as in the interpretation of the results. They also critically reviewed the paper, approved its final version and agreed with its publication.

– No signature responsible for the work has been omitted and the criteria of Scientific Authorization are satisfied.

– The results of this Article have been interpreted objectively. Any results contrary to the point of view of those who sign are exposed and discussed in the Article.

Copyright and Access

The publication of this Article supposes the transfer of the copyright to ECORFAN-Mexico, SC in its Holding Spain for its Journal of Research and Development, which reserves the right to distribute on the Web the published version of the Article and the making available of the Article in This format supposes for its Authors the fulfilment of what is established in the Law of Science and Technology of the United Mexican States, regarding the obligation to allow access to the results of Scientific Research.

Article Title:

Name and Surnames of the Contact Author and the Coauthors	Signature
1.	
2.	
3.	
4.	

Principles of Ethics and Declaration of Solution to Editorial Conflicts

Editor Responsibilities

The Publisher undertakes to guarantee the confidentiality of the evaluation process, it may not disclose to the Arbitrators the identity of the Authors, nor may it reveal the identity of the Arbitrators at any time.

The Editor assumes the responsibility to properly inform the Author of the stage of the editorial process in which the text is sent, as well as the resolutions of Double-Blind Review.

The Editor should evaluate manuscripts and their intellectual content without distinction of race, gender, sexual orientation, religious beliefs, ethnicity, nationality, or the political philosophy of the Authors.

The Editor and his editing team of ECORFAN® Holdings will not disclose any information about Articles submitted to anyone other than the corresponding Author.

The Editor should make fair and impartial decisions and ensure a fair Double-Blind Review.

Responsibilities of the Editorial Board

The description of the peer review processes is made known by the Editorial Board in order that the Authors know what the evaluation criteria are and will always be willing to justify any controversy in the evaluation process. In case of Plagiarism Detection to the Article the Committee notifies the Authors for Violation to the Right of Scientific, Technological and Innovation Authorization.

Responsibilities of the Arbitration Committee

The Arbitrators undertake to notify about any unethical conduct by the Authors and to indicate all the information that may be reason to reject the publication of the Articles. In addition, they must undertake to keep confidential information related to the Articles they evaluate.

Any manuscript received for your arbitration must be treated as confidential, should not be displayed or discussed with other experts, except with the permission of the Editor.

The Arbitrators must be conducted objectively, any personal criticism of the Author is inappropriate.

The Arbitrators must express their points of view with clarity and with valid arguments that contribute to the Scientific, Technological and Innovation of the Author.

The Arbitrators should not evaluate manuscripts in which they have conflicts of interest and have been notified to the Editor before submitting the Article for Double-Blind Review.

Responsibilities of the Authors

Authors must guarantee that their articles are the product of their original work and that the data has been obtained ethically.

Authors must ensure that they have not been previously published or that they are not considered in another serial publication.

Authors must strictly follow the rules for the publication of Defined Articles by the Editorial Board.

The authors have requested that the text in all its forms be an unethical editorial behavior and is unacceptable, consequently, any manuscript that incurs in plagiarism is eliminated and not considered for publication.

Authors should cite publications that have been influential in the nature of the Article submitted to arbitration.

Information services

Indexation - Bases and Repositories

LATINDEX (Scientific Journals of Latin America, Spain and Portugal)
EBSCO (Research Database - EBSCO Industries)
RESEARCH GATE (Germany)
GOOGLE SCHOLAR (Citation indices-Google)
REDIB (Ibero-American Network of Innovation and Scientific Knowledge- CSIC)
MENDELEY (Bibliographic References Manager)

Publishing Services

Citation and Index Identification H
Management of Originality Format and Authorization
Testing Article with PLAGSCAN
Article Evaluation
Certificate of Double-Blind Review
Article Edition
Web layout
Indexing and Repository
ArticleTranslation
Article Publication
Certificate of Article
Service Billing

Editorial Policy and Management

38 Matacerquillas, CP-28411. Moralzarzal –Madrid-España. Phones: +52 1 55 6159 2296, +52 1 55 1260 0355, +52 1 55 6034 9181; Email: contact@ecorfan.org www.ecorfan.org

Journal of Research and Development

2444 4987
ISSN 2444 - 4987

www.ecorfan.org